# Effects of Initial Soil Moisture on Rainfall Generation and Subsequent Hydrologic Response during the North American Monsoon

By

Kinwai Tai

Submitted in Partial Fulfillment of Requirements for the

Degree of Master of Science in Hydrology

Department of Earth and Environmental Science

New Mexico Institute of Mining and Technology

Socorro, New Mexico

June 2008

To my mother, wife and in memory of my devoted father

## ABSTRACT

A moderate change in soil moisture condition typically alters the intensity, location and timing of convective rainfall. From a meteorological point of view, studying the soil moisture-rainfall relationship is important for understanding rainfall generation and enhancing rainfall predictability. In the hydrological community, soil moisture plays an important role in shaping hydrologic responses which are influenced by rainfall variability and watershed antecedent wetness conditions. The interaction among soil moisture, rainfall and hydrologic response motivates us to study the effect of initial soil moisture on rainfall generation and subsequent hydrologic response in the North American Monsoon (NAM) region. To conduct our study, we couple the Weather Research and Forecasting (WRF) model to the Triangulated Irregular Network (TIN)-based Real-time Integrated Basin Simulator (tRIBS) hydrologic model in a one-way, off-line mode. Our particular case study focuses on a four-day warm-season mesoscale convective storm event occurring over the Upper Río Puerco in the north central New Mexico. To understand the impact of initial soil moisture variations on rainfall generation in the NAM region, we used the WRF meteorological model to simulate an ensemble of meteorological fields by systematically varying the soil moisture initialization in the model domains. The intercomparsion of the ensemble basin-scale rainfall simulations shows that the total rainfall volume increases with increasing initial soil moisture to an upper limit in our warm-season case study. We then use the ensemble meteorological fields to force the

tRIBS model using two different scenarios: (1) fixed soil moisture initializations in tRIBS; and (2) adjusted soil moisture initializations between WRF and tRIBS (for the Upper Río Puerco watershed). The results indicate that the runoff ratio increases with increasing rainfall volume but the trend is more pronounced and nonlinear in the adjusted initialization cases. These differences suggest that the runoff response is primarily driven by rainfall intensity in the fixed initialization, while it is the result of both rainfall intensity and antecedent wetness in the adjusted initialization. The antecedent soil moisture condition significantly shapes the runoff response through the partitioning between different runoff mechanisms and also impacts the partitioning of surface turbulent fluxes and the return of water vapor back to the atmosphere via evapotranspiration. Our high resolution and distributed modeling approach is an early attempt to understand the impact of soil moisture initializations on rainfall production, streamflow response and evapotranspiration. We conclude that increases in initial soil moisture conditions promote an increase in rainfall, runoff production and latent heat flux in our warm-season case study. As a result, proper soil moisture initializations in both meteorological and hydrological models should lead to improved hydrometeorological predictions.

ACKNOWLEDGEMENTS

I would like to thank my advisor, Dr. Enrique Vivoni and my committee, Dr. David Raymond and Dr. John Wilson for their guidance and inspiration that enriched this M.S. thesis. I also appreciate intellectual suggestions from former and current research group members of Dr. Vivoni during my studies at New Mexico Institute of Mining and Technology.

Warm thanks are extended to Dr. David Gochis, Wei Yu and Dr. Joe Galewsky for their guidance with respect to the atmospheric modeling research. Additional thanks to National Center for Atmospheric Research for their technical and computing assistance of meteorological simulations.

Finally, I am deeply indebted to my family. My parents had worked diligently in all their lives to support a better growth and future for their children.

TABLE OF CONTENTS


| SECTION | TITLE | PAGE |
|---|---|---|
| LIST OF FIGURES | | v |
| LIST OF TABLES | | ix |
| CHAPTER 1: | INTRODUCTION | 1 |
| 1.1 | Background and Motivation | 1 |
| 1.2 | Summary of Models | 4 |
| 1.3 | Overview of Thesis | 6 |
| CHAPTER 2: | EFFECTS OF INITIAL SOIL MOISTURE ON RAINFALL GENERATION AND SUBSEQUENT HYDROLOGIC RESPONSE DURING THE NORTH AMERICAN MONSOON | |
| 2.1 | Introduction | 8 |
| 2.2 | Methods | 13 |
| 2.2.1 | Study Area | 13 |
| 2.2.2 | Atmospheric Model: WRF | 21 |
| 2.2.3 | Distributed Hydrological Model: tRIBS | 18 |
| 2.2.4 | Numerical Experiment | 29 |
| 2.3 | Results and Discussion | 30 |
| 2.3.1 | Effect of Initial Soil Moisture on Basin-Scale Rainfall Properties | 30 |
| 2.3.2 | Effect of Rainfall Forcing on Hydrologic Response under Fixed Initializations | 40 |
| 2.3.3 | Effect of Rainfall Forcing on Hydrologic Response under Adjusted Initializations | 45 |
| 2.3.4 | Effect of Soil Moisture Initialization on Evapotranspiration Response | 54 |
| 2.4 | Conclusions | 60 |
| CHAPTER 3: | SUMMARY AND RECOMMENDATIONS | |
| 3.1 | Summary | 63 |

| | | |
|---|---|---|
| 3.2 | Recommendations for Future Work | 66 |
| REFERENCES | | 68 |
| APPENDICES | | 78 |
| A.1 | Outline of Data Structure | 78 |
| A.2 | WRF Preprocessing System (WPS) | 79 |
| A.3 | WRF Model Simulations | 80 |
| A.4 | tRIBS for the Fixed Initializations | 83 |
| A.5 | tRIBS for the Adjusted Initializations | 87 |
| A.6 | IDL Script for Postporcessing WRF output for tRIBS | 92 |

LIST OF FIGURES


| FIGURE | CAPTION | PAGE |
|---|---|---|
| 2.1 | Study site represented at different modeling scales. (a) Nested domains for Weather Research and Forecasting (WRF) model. Domain 1 (D01) consists of 30-km coarse grid spacing and contains the western US, followed by nested Domain 2 (D02) with 10-km grid spacing; while Domain 3 (D03) consists of ~3.33-km finer grid spacing and is focused on the Four Corners region. (b) Location of Río Puerco basin in north central New Mexico within D03. In this study, we focused the hydrological modeling efforts in the Upper Río Puerco (c) above the USGS gauge (Río Puerco above Arroyo Chico near Guadalupe, NM). The topographic domain in the basin consists of a north-to-south trending mountain front (Nacimiento Mountains) along the eastern border. | 14 |
| 2.2 | Rainfall hyetograph (top-axis) and streamflow hydrograph (bottom-axis) in the Upper Río Puerco basin. The radar rainfall hyetograph (mm/hr) represents the basin-averaged rainfall rate obtained from the 4-km NEXRAD (Stage III) hourly data. Discharge hydrograph ($m^3/s$) is shown for the USGS gauging station in the Upper Río Puerco basin above Arroyo Chico Near Guadalupe. Note that the peak discharge is ~50 $m^3/s$. The time to peak was computed based on the rainfall centroid, yielding a value of ~1 day. The runoff ratio was also computed using the flood volume at the gauge ($4.48 \times 10^6$ $m^3$) and the radar rainfall volume ($4.20 \times 10^7$ $m^3$), yielding a value of 0.106 (10.6%) for the flood event (Vivoni et al. 2006). | 16 |
| 2.3 | Effect of the soil moisture multiplier ($\alpha$ = 0.0 and 2.25) on the initial volumetric soil moisture ($m^3/m^3$) in WRF for the top layer (0 to 10 cm in depth) in each domain. | 19 |
| 2.4 | Effect of the soil moisture multiplier ($\alpha$, ranging from 0 to 2.25) on the initial soil moisture field in WRF for the top layer (0 to 10 cm in depth) in each domain. The statistical properties of the initial soil moisture for (a) Domain 1, (b) | |

Domain 2, and (c) Domain 3 include the minimum, maximum, and spatial mean volumetric soil moisture ($m^3/m^3$) with ± 1 standard deviation of the spatial soil moisture ($m^3/m^3$). 20

2.5 Spatial distribution of the (a) surface soil texture classification (STATSGO), (b) land use or vegetation type (NLCD), (c) the initial depth to groundwater table (mm) and (d) the initial surface soil moisture ($m^3/m^3$) for the fixed initialization for the Upper Rio Puerco basin as represented in the tRIBS distributed hydrological model. 25

2.6 Spatial distribution of the initial surface soil moisture ($m^3/m^3$) for the adjusted initialization cases for the Upper Rio Puerco basin as represented in the tRIBS distributed hydrological model. Only a selected number of $\alpha$ cases are shown for clarity. 28

2.7 Rainfall comparison between NEXRAD Stage III product (4-km, 1-hr resolutions) and WRF control simulation ($\alpha$=1, 3.3-km, 1-hr resolutions) for (a) the spatial distribution of total storm rainfall (mm), and (b) the temporal distribution of basin-averaged rainfall rate (mm/hr). 32

2.8 Comparison of the hourly basin-averaged rainfall rate (mm/hr) for different initial soil moisture conditions ($\alpha$ = 0 to 2.25) in the WRF model over the Upper Río Puerco. The horizontal dashed lines represent the temporal mean of the basin-averaged rainfall. Note that increasing $\alpha$ occurs along columns from top to bottom. 33

2.9 Comparison of the basin rainfall coverage ($A_R$ in %) depicted as the percentage of total basin area with rainfall greater than zero. The horizontal dashed lines represent the temporal mean of the basin rainfall coverage. 35

2.10 Comparison of the spatial distributions of total rainfall accumulation during the storm period (mm), September 8-12, 2003, for the different initial soil moisture conditions ($\alpha$). 37

2.11 Impact of the initial soil moisture multiplier on rainfall field statistics over the Upper Río Puerco. (a) Total rainfall volume ($m^3$). (b) Maximum of basin-averaged hourly rainfall (mm/hr). (c) Maximum of pixel-scale rainfall rate

(mm/hr). (d) Total length of time with rainfall coverage at 100% of basin area (hr). 38

2.12 Comparison of basin hydrologic response for simulations with different WRF initial soil moisture ($\alpha$ = 0 to 2.25) and fixed initial soil moisture conditions in tRIBS. (a) Cumulative basin-averaged rainfall volume ($m^3$). (b) Basin-averaged mean surface soil moisture (in top 10 cm), expressed as relative saturation ($s = \theta / n$); $\theta$ is the volumetric soil moisture content ($m^3/m^3$) and $n$ is the soil porosity. (c) Cumulative discharge ($m^3$) at the Upper Río Puerco basin outlet. Note that the USGS streamflow observations, the NEXRAD forcing and its associated hydrological response based on model simulations is included for comparison purposes. The ensemble mean over the 16 different cases is shown with the solid black lines. 41

2.13 Spatial distributions of the percent of time with infiltration-excess runoff occurrence (%) during September 8-16, 2003, for the fixed initial soil moisture conditions. 44

2.14 Comparison of basin hydrologic response for simulations with adjusted initial soil moisture conditions in tRIBS and WRF ($\alpha$ = 0.75 to 2.25). (a) Cumulative basin-averaged rainfall volume ($m^3$). (b) Basin-averaged mean surface soil moisture (in top 10 cm), expressed as relative saturation ($s = \theta / n$); $\theta$ is the volumetric soil moisture content ($m^3/m^3$) and $n$ is the soil porosity. (c) Cumulative discharge ($m^3$) at the Upper Río Puerco basin outlet. 48

2.15 Spatial distributions of the percent of time with saturation-excess runoff occurrence (%) during September 8-16, 2003, for the adjusted initial soil moisture conditions. 51

2.16 Effect of rainfall volume on the runoff response. (a) Basin runoff ratio ($r = Q/P$) in Upper Río Puerco outlet for fixed initialization (16 cases) and adjusted initialization (13 cases). (b) Runoff contributions from individual runoff mechanisms as percentage of total runoff (%). Runoff mechanisms include infiltration-excess, saturation-excess, perched return flow and groundwater exfiltration. The runoff contributions are only shown for the adjusted soil moisture initializations between WRF and tRIBS since the fixed initialization yields 100% infiltration-excess runoff for all simulations. 53

2.17 Comparison of basin-averaged evapotranspiration ($m^3$) for: (a) simulations with different WRF initial soil moisture ($\alpha$ = 0 to 2.25) and fixed initial soil moisture conditions in tRIBS and (b) simulations with adjusted initial soil moisture conditions in tRIBS and WRF ($\alpha$ = 0.75 to 2.25). 56

2.18 Effect of rainfall volume on basin evapotranspiration (ET). (a) Total evapotranspiration volume ($m^3$) for fixed (16 cases) and adjusted initializations (13 cases). The labeled cases ($\alpha$ = 0.75, 1.00, 1.25, 1.75 and 2.25) correspond to those presented in Figure 2.17. (b) Evapotranspiration ratio in % (*ET*/*P*) for the two scenarios. 57

2.19 Effect of initial soil moisture conditions on the evaporative fraction (-) for fixed (left column) and adjusted (right column) initializations. Only a selected number of $\alpha$ cases are shown for clarity. 59

LIST OF TABLES


| TABLE | CAPTION | PAGE |
|---|---|---|
| 2.1 | Land cover parameter values for the Upper Río Puerco in the calibrated tRIBS distributed hydrologic model. $A$ is the percentage of basin area of this particular land cover type (%); $P$ is the free throughfall coefficient (-); $S$ is the canopy field capacity (mm); $K$ is the drainage coefficient (mm/hr); $g$ is the drainage exponential parameter ($mm^{-1}$); $Al$ is the albedo (-); $h$ is the vegetation height (m); $K_t$ is the optical transmission coefficient (-); $R_s$ is the canopy-average stomatal resistance (s/m); and $V$ is the vegetation fraction. | 23 |
| 2.2 | Soil parameter values for the Upper Río Puerco in the calibrated tRIBS distributed hydrologic model. $A$ is the percentage of basin area of this particular soil type (%); $K_s$ is the saturated hydraulic conductivity (mm/hr); $\Theta_s$ is the soil moisture at saturation (-); $\Theta_r$ is the residual soil moisture (-); $m$ is the pore distribution index (-); $\psi_b$ is the air entry bubbling pressure (mm); $f$ is the conductivity decay parameter ($mm^{-1}$); $A_s$ is the saturated anisotropy ratio (-); $A_u$ is the unsaturated anisotropy ratio (-); and $n$ is the porosity (-). | 24 |
| 2.3 | The mean and standard deviation of the depth to initial groundwater table (mm) and basin-averaged volumetric soil moisture ($m^3/m^3$) for each adjusted initialization ($\alpha$). | 47 |
| A.1 | Input datasets in WPS. | 79 |
| A.2 | Model output datasets in the WPS. | 79 |
| A.3 | Input datasets in WRF. | 81 |
| A.4 | Model output datasets in WRF. | 82 |
| A.5 | Model run files for tRIBS simulations with fixed initializations. | 83 |

A.6 Input datasets for tRIBS simulations with fixed initializations. 84

A.7 Meteorological inputs for tRIBS simulations with fixed initializations. 85

A.8 Model output datasets for tRIBS simulations with fixed initializations. 86

A.9 Model run files for tRIBS simulations with adjusted initializations. 87

A.10 Input datasets for tRIBS simulations with adjusted initializations. 88

A.11 Initial groundwater inputs for tRIBS simulations with adjusted initializations. 89

A.12 Meteorological inputs for tRIBS simulations with adjusted initializations. 90

A.13 Model output datasets for tRIBS simulations with adjusted initializations. 91

This thesis is accepted on behalf of the
Faculty of the Institute by the following committee:

Enrique R. Vivoni

Advisor

John L. Wilson

David G. Raymond

6-16-08

Date

I release this document to the New Mexico Institute of Mining and Technology.

Student's Signature

6-16-2008

Date

# CHAPTER 1: INTRODUCTION

## 1.1 Background and Motivation

Understanding the effect of soil moisture initialization on rainfall generation has been hypothesized to contribute skill to warm-season climate prediction in the NAM region (e.g., Beljaars et al. 1996; Higgins et al. 2003; Vera et al. 2006; Gao et al. 2007). In particular, a moderate soil moisture variation can typically change the location and timing of convective rainfall that significantly affects the forecasting skills for short-range weather (Benjamin and Carlson 1986; Lanicci et al. 1987; Sutton et al. 2006). In order to improve forecasting skill, a prime focus should be on studying the relationship between soil moisture perturbations and rainfall variability. While this is somewhat deterred in operation, due to the lack of extensive soil moisture observational data, numerical models can nonetheless be operated as a laboratory for examining rainfall variability induced by the realizations of varying antecedent soil moisture conditions.

In addition to the impact of soil moisture specification on weather prediction, the soil moisture-rainfall relationship also significantly influences hydrological forecasting of summer flood events in the NAM region. Studies have presented inaccurate runoff simulations from hydrometeorological modeling systems (e.g., Chancibault et al. 2006; Hay et al. 2006), suggesting that a challenge exists in accurately simulating spatiotemporal rainfall distributions required for hydrological models. For example, Hay et al. (2006) compared predictions from a one-way

coupling of atmospheric and hydrologic models to runoff simulations based on forcing the hydrologic model with climate station data. They found that a primary cause for low streamflow predictability using the hydrometeorological models was the propagation of errors in the meteorological simulations, particularly the spatiotemporal rainfall distributions, into the hydrologic model. Moreover, studies by Decharme and Douville (2006) and Lin et al. (2006) also concluded that uncertainty in simulated rainfall forcing significantly impacts hydrologic simulations.

These studies motivate a research effort required to understand the basin hydrologic response and its sensitivity to various meteorological simulations. To carry out this research effort, a meteorological model can be used as a systematic tool for creating an ensemble of rainfall fields based on the variation of initial or boundary conditions. For example, a regional climate model can simulate spatially distributed rainfall fields at high resolution (~1 km spatial and ~15 min temporal resolutions), which can be used as forcing for a hydrological model to simulate detailed water and energy fluxes in the land surface (Westrick and Mass 2001; Seuffert et al. 2002; Hay et al. 2006). In this regard, distributed hydrologic models are sophisticated tools for this effort because they account for detailed representations of hydrologic processes and utilize fine-scale descriptors such as vegetation, topography and soil properties. This distributed capability has been shown to be a distinctive advantage over conceptual, lumped models used widely for streamflow and flood forecasting (e.g., Reed et al. 2004; Ivanov et al. 2004a; Vivoni et al. 2007c). In this study, a distributed hydrological model is used based on its capacity to transform meteorological forcing into detailed land surface states and fluxes, such as soil moisture and

evapotranspiration, in addition to streamflow predictions at multiple locations along a channel network.

To understand the hydrologic sensitivity to the initial soil moisture conditions in a meteorological simulation, we force a distributed hydrological model with an ensemble of meteorological model fields. To achieve this, we couple a fully-distributed hydrological model to a nested domain meteorological model in a one-way, offline mode. Meteorological fields at the land surface (e.g. rainfall, surface pressure, air temperature, relative humidity, and wind speed distributions) are used to force the distributed model at a high spatiotemporal resolution over a relatively short forecast period.

The main objectives of this thesis are to: (1) use a systematic method to generate an ensemble of meteorological fields by varying the soil moisture initialization, (2) analyze the rainfall characteristics simulated by the meteorological model under various soil moisture scenarios, and (3) evaluate the basin hydrological response to the ensemble of meteorological forcings under a different set of conditions. In particular, we explore the differences in basin response induced by varying the antecedent soil moisture condition (to match the meteorological model initialization). Based on a comparison between the simulated rainfall of a base meteorological simulation case, (which is induced by unchanged initial soil moisture) and radar rainfall observations, this base case produces reasonable rainfall simulation and thus somewhat corresponds to realism of the nature. However, a sensitivity analysis to varying soil moisture initializations from the base meteorological simulation case is a synthetic study. This high resolution and distributed modeling

approach is an early attempt to understand the impact of soil moisture on rainfall and subsequent streamflow predictability.

This thesis is organized as follows. A brief description of the meteorological and hydrological models for this study is presented in the following paragraph, followed by a description of each chapter in the thesis. A manuscript describing the experimental design, research questions, corresponding results and conclusions is presented in Chapter 2. In Chapter 3, we provide concluding remarks and recommendations for future work, followed by an appendix for supplementary documentation.

### 1.2 Summary of Models

The atmospheric model utilized for this study is the Weather Research and Forecasting (WRF) Advanced Research WRF (ARW) model. It is a nonhydrostatic, Eulerian mesoscale model (Skamarock et al. 2005) that has been used widely for research and forecasting purposes. The WRF model is an open source code which is being developed and maintained by National Center for Atmospheric Research (NCAR), other universities, government and research agencies. It is composed of a state-of-the-art, flexible, portable code that can be efficiently operated in a massively parallel computing environment. For this study, we performed all the WRF simulations in a high performance computing cluster (64-processors) at New Mexico Tech. WRF consists of numerous physics options benefiting a broad modeling community. It offers a spectrum of applications across scales ranging from meters to thousands of kilometers. For example, such applications cover research and

operational numerical weather prediction (NWP), atmosphere-ocean coupling, downscaling climate simulations, data assimilation research and idealized simulations (e.g., convection, baroclinic wave and boundary-layer eddies).

The Triangulated Irregular Network (TIN)-based Real-time Integrated Basin Simulator (tRIBS) is a physically based, fully-distributed hydrological model designed to operate with meteorological forcing from rain gauges, weather radar or numerical weather prediction models (e.g., Ivanov et al. 2004a,b, Vivoni et al. 2005, 2007b). Simulation of the coupled surface and groundwater response to the meteorological fields is performed by analyzing infiltration fronts, water table fluctuations and lateral moisture fluxes in the vadose and saturated zones depending on vegetation, soil and aquifer properties (e.g., Vivoni et al. 2006, 2007c). Surface runoff is simulated via four different mechanisms: infiltration-excess, saturation-excess, perched subsurface stormflow and groundwater exfiltration. Routing of surface flow is done through hydraulic channel routing and hydrologic overland flow (see Ivanov et al. 2004a). Evapotranspiration is composed of bare soil evaporation, vegetation transpiration, and evaporation of intercepted rainfall which require radiation and energy balance calculations using estimates of the surface meteorological conditions. The tRIBS model is a hydrologic research and flood forecasting model which is under a continuous development by researchers at Massachusetts Institute of Technology and New Mexico Institute of Mining and Technology. It is written in C++ code designed for distributed hydrologic modeling at small (meters) to mid-size catchment (thousands of kilometers) scales. For this study,

we performed all the tRIBS simulations serially in a high performance computing cluster (64-processors) at New Mexico Tech.

### 1.3 Overview of Thesis

This thesis is written to present (1) the effect of initial soil moisture condition on rainfall generation and subsequent hydrologic response; (2) the influence of antecedent soil moisture condition on various runoff mechanisms and evapotranspiration response.

The second chapter is organized in paper format for a submission to the *Journal of Hydrometeorology*. The paper is titled *Effects of Initial Soil Moisture on Rainfall Generation and Subsequent Hydrologic Response during the North American Monsoon.* The paper focuses on the role of antecedent soil moisture condition on rainfall-runoff production and evapotranspiration. In particular, we attempt to demonstrate the influence of soil moisture initialization on runoff production through various runoff mechanisms. In this chapter, we present an introduction to some general issues (i.e. impact of soil moisture) associated with rainfall and streamflow processes and predictions. We then present the study area, the Upper Río Puerco (URP) basin in north central New Mexico; introduce a case study related to a four-day warm-season mesoscale convective storm during the late monsoon season of September 2003; review the meteorological and hydrologic models; and describe the approach for our numerical experiment. In Section 2.2.1, we present and compare the WRF ensemble rainfall simulations induced by different soil moisture initializations. This intercomparsion result demonstrates the effect of antecedent soil moisture condition on rainfall generation. In the Sections 2.2.2 and

2.2.3, we compare the results of ensemble hydrological simulations based upon two different scenarios: (1) fixed soil moisture initializations in tRIBS; and (2) adjusted soil moisture initializations between WRF and tRIBS. These results are synthesized and discussed by examining the significance of antecedent wetness on various runoff mechanisms on runoff generation and evapotranspiration. In the Section 3, we summarize the implications of the results.

Chapter 3 presents a summary of the conclusions and recommendations for future studies. The Appendix documents the input and output datasets for all the ensemble simulations from WRF and tRIBS included in a data storage machine called "CRIB (/model-out)" at New Mexico Tech. This is included in such as way that the model simulations can serve for future studies or reference purposes.

# CHAPTER 2: EFFECTS OF INITIAL SOIL MOISTURE ON RAINFALL GENERATION AND SUBSEQUENT HYDROLOGIC RESPONSE DURING THE NORTH AMERICAN MONSOON

## 2.1 Introduction

Atmospheric initialization including soil moisture conditions in the land surface can significantly affect the performance of weather and flood forecasts (e.g., Mahfouf 1991; Beljaars et al. 1996; Schar et al. 1999). Various studies have indicated a strong effect of soil moisture on rainfall (Mintz 1984; Mo et al. 2006; Aligo et al. 2007) and as a result a proper initialization of soil moisture conditions would enhance the predictability of rainfall (Miyakoda et al. 1979; Beljaars et al. 1996; Schar et al. 1999; Seuffert et al. 2002; Wang et al. 2007). This is especially valid for regions of strong coupling between rainfall and soil moisture such as transitional areas between dry and wet climates (Koster et al. 2004). One of those transition regions is southwestern United States where summertime convective rainfall is promoted and where evapotranspiration is sensitive to soil moisture conditions during the North American monsoon (NAM) (e.g., Hong and Pan 2000; Pal and Eltahir 2001; Matsui et al. 2005; Kurc and Small 2007; Vivoni et al. 2007a). High soil moisture conditions tend to lower land surface albedo and the Bowen ratio (i.e., ratio of sensible to latent heat flux), which in turn increase the net surface radiation and the total heat flux from the land surface (e.g., Zheng and Eltahir 1998a; Eltahir 1998). The increase of total heat flux promotes a larger boundary layer moist static energy and increased rainfall

through the additional local evapotranspiration and large-scale moisture convergence (Eltahir 1998; Pal and Eltahir 2001).

In numerical models, soil moisture conditions and the physical parameterizations related to convection may dictate the magnitude of rainfall anomalies (e.g., Xu and Small 2002; Gochis et al. 2002; Gochis et al. 2003; Ratnam and Kumar 2005). For example, numerical studies by Small (2001) and Xu et al. (2004) demonstrated a positive soil moisture-rainfall feedback in the NAM region during the summertime (i.e., lower soil moisture leads to lower rainfall and vice-versa). Soil moisture has also been linked to the NAM onset, as wet winter and spring conditions reduce the land-sea thermal contrast and delay the monsoon (Zhu et al. 2007). Numerical studies in other regions (e.g., Bosilovich and Sun 1999; Hong and Pan 2000; Pal and Eltahir 2001; Oglesby et al. 2002; Schubert et al. 2004; Kim and Wang 2007a) have also found a positive feedback between soil moisture and rainfall. This relation, however, may only be valid under a certain range of perturbations in the soil moisture field, which have not been clearly investigated to date. The strength of this feedback is also likely to depend on the geographic location and season of interest. For example, the soil moisture-rainfall feedback is thought to be particularly pronounced during the summertime (Schar et al. 1999; Hong and Pan 2000) and for transition regions between dry and wet climates (Koster et al. 2004; Wang et al. 2007).

Understanding the circumstances under which soil moisture impacts rainfall has been hypothesized to contribute skill to warm-season climate prediction in the NAM region (e.g., Beljaars et al. 1996; Higgins et al. 2003; Vera et al. 2006; Gao et

al. 2007). For example, a moderate change in the soil moisture condition tends to alter the location and timing of convective rainfall leading to a significant impact on short-range weather forecasting (Lanicci et al. 1987; Sutton et al. 2006). Therefore, more attention should be allocated to studying the relationship between soil moisture perturbations and rainfall variability. Although this is hampered by the lack of extensive soil moisture observational data, numerical models can nevertheless be used as a laboratory for investigating rainfall variability induced by realizations of different initial or concurrent soil moisture conditions.

The soil moisture-rainfall feedback also has important implications on hydrological forecasting of summer flood events at the watershed scale in the NAM region. Recent studies have shown that streamflow predictions using hydrometeorological modeling systems can yield inaccurate runoff simulations (e.g., Chancibault et al. 2006; Hay et al. 2006), suggesting the difficulty in capturing the space-time rainfall distributions at the scales required for hydrological models. For example, Hay et al. (2006) compared predictions from a one-way coupling of atmospheric and hydrologic models to those runoff simulations based on simply forcing the hydrologic model with climate station data. One of the major causes identified for low streamflow predictability using the hydrometeorological models was the propagation of spatiotemporal rainfall forecast errors into the hydrologic model response. Studies by Decharme and Douville (2006) and Lin et al. (2006) also concluded that uncertainty in simulated rainfall forcing significantly impacts hydrologic simulations.

These studies indicate that additional effort is required to understand the basin hydrologic response and its sensitivity to different synthetic meteorological simulations. For this purpose, an atmospheric model is a systematic tool for generating an ensemble of rainfall fields based on the variation of initial or boundary conditions. A regional climate model, for example, can simulate spatially distributed rainfall fields at high resolution (~1 km spatial and ~15 min temporal resolutions), which can be used effectively as forcing to simulate the water and energy fluxes in the land surface (Westrick and Mass 2001; Seuffert et al. 2002; Hay et al. 2006). To take advantage of these high resolution forecasts, distributed hydrologic models accounting for detailed representations of hydrological processes are needed as these models utilize fine-scale basin descriptors such as topography, vegetation and soil properties. This distributed capability has been shown to be a distinctive advantage over conceptual, lumped models used widely for streamflow and flood forecasting (e.g., Reed et al. 2004; Ivanov et al. 2004a; Vivoni et al. 2007c). The capacity of a distributed hydrologic model to transform meteorological forcing into detailed land surface states and fluxes, such as soil moisture, runoff production and evapotranspiration, motivates their use in hydrometeorological forecasting systems.

In this study, we perform a sensitivity study of the simulated hydrologic response using an ensemble of meteorological forcings generated by varying the initial soil moisture conditions over a large semiarid region. To do so, we couple a nested domain atmospheric model to a fully-distributed hydrological model in a one-way, offline mode. Meteorological fields at the land surface (e.g., air temperature, pressure, humidity, wind, and rainfall distributions) are used to force a distributed

hydrological model at a high spatiotemporal resolution over a relatively short forecast period (~4 days) covering a major storm and flood event. According to NEXRAD rainfall observations, rainfall only occurred in the first 4-day period (8-12 September, 2003). To achieve that, we perform the meteorological simulations only for this first 4-day period and avoid a potential problem of simulated rainfall after the 4-day period induced by synthetic wet antecedent soil moisture conditions in the meteorological model. To ensure the majority of streamflow generated by the 4-day rainfall event leaving through the basin outlet, we perform the hydrological simulations for an 8-day period (8-16 September, 2003). Because of the need of atmospheric forcings for the 8-day hydrological simulations, we manually generate the atmospheric forcings for the last 4 days (12-16 September, 2003) using zero rainfall padding and replicating the diurnal meteorological data from the first day of the WRF simulation which exhibited relatively clear conditions. The main objectives of this paper are to: (1) use a systematic method to generate an ensemble of meteorological fields by varying initial soil moisture conditions, (2) analyze the rainfall characteristics simulated by the atmospheric model under various soil moisture scenarios, and (3) evaluate the basin hydrological response to the ensemble of meteorological forcings under a different set of initializations. In particular, we explore the differences in basin response induced by varying the antecedent moisture condition in the hydrologic model to match the atmospheric model initialization. This high resolution and distributed modeling approach is an early attempt to understand the impact of soil moisture on rainfall and subsequent streamflow predictability and evapotranspiration in the North America monsoon region.

The paper is organized as follows. A brief description of the study area is presented in section 2.2, followed by a description of the atmospheric and hydrological models and the experimental setup for the numerical simulations. Results from the numerical experiments are presented and discussed in section 2.3. We emphasize the impact of soil moisture perturbations on the simulated rainfall field and basin streamflow response and evapotranspiration for a large convective event in the southwestern United States. Particular focus is placed on how the soil moisture-induced rainfall fields interact with different scenarios of the watershed hydrologic initial condition. Finally, we present conclusions in section 2.4.

## 2.2 Methods

### 2.2.1 Study Area

The site selected for this study is the Upper Río Puerco (URP) basin, located in north central New Mexico (Figure 2.1). We delineated the Upper Río Puerco basin based on a United States Geological Survey (USGS) 30-m Digital Elevation Model (DEM) using the hydrographic Triangulated Irregular Network (TIN) procedure described in Vivoni et al. (2004). We also delineated a stream network with drainage density of 0.25 $km^{-1}$ by comparisons against the 1 m orthophotos of the region obtained from the New Mexico Resource Geographic Information System Program (http://rgis.unm.edu). The 1117-$km^2$ basin has a range of elevation from 1802 m to 3222 m with the Nacimiento Mountains along the eastern watershed divide and decreasing elevations toward the basin outlet. The Upper Río Puerco basin is characterized by a mixture of land use: forest (39%), shrubland (29%) and grassland (29%). The soil texture is primarily loam (43%), clay loam (33%), sandy loam (16%),

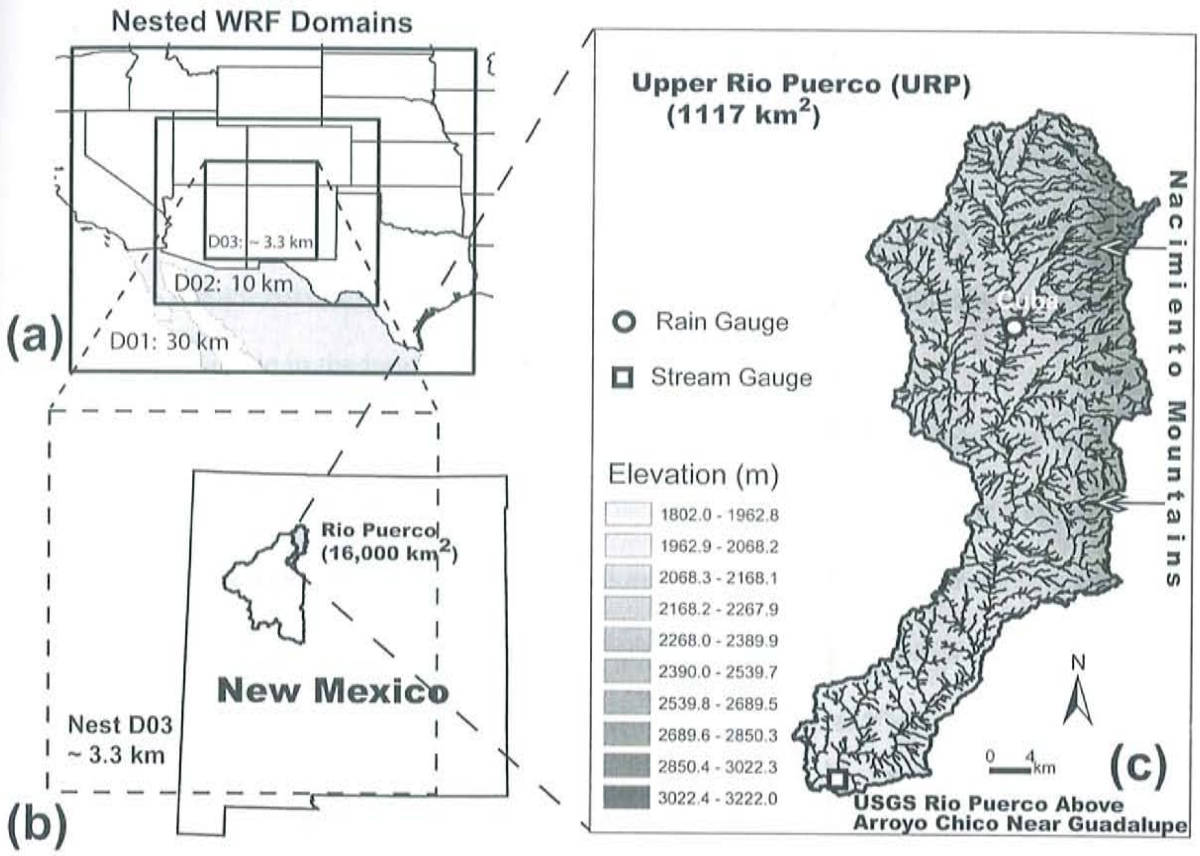


**Figure 2.1.** Study site represented at different modeling scales. (a) Nested domains for Weather Research and Forecasting (WRF) model. Domain 1 (D01) consists of 30-km coarse grid spacing and contains the western US, followed by nested Domain 2 (D02) with 10-km grid spacing; while Domain 3 (D03) consists of ~3.33-km finer grid spacing and is focused on the Four Corners region. (b) Location of Río Puerco basin in north central New Mexico within D03. In this study, we focused the hydrological modeling efforts in the Upper Río Puerco (c) above the USGS gauge (Río Puerco above Arroyo Chico near Guadalupe, NM). The topographic domain in the basin consists of a north-to-south trending mountain front (Nacimiento Mountains) along the eastern border.

unweathered bedrock (7%) and silt loam (~1%). A long-term rain gauge site is located within the Upper Río Puerco at Cuba, NM. Being a semiarid environment, the URP receives an average total annual rainfall of 323 mm/yr at Cuba (Griffin et al. 2005). Streamflow at the basin outlet is measured by a USGS stream gauge (Río Puerco Above Arroyo Chico near Guadalupe, NM). Other hydrological observations are not available in the largely rural, semiarid basin.

Vivoni et al. (2006) studied a major storm event that occurred during September 8-12, 2003 in the Río Puerco based on NEXRAD, rain gauge and stream gauge observations. The large monsoon storm developed over Arizona and moved into New Mexico, resulting in high rainfall accumulations and a major flood associated with a series of convective storm cells. Figure 2.2 presents the basin-averaged rainfall and flood response for this summer monsoon event. We selected this period for the detailed numerical modeling due to the extended rainfall area and duration and the significant flood response. The large size and duration of the monsoon storm possibly leads to greater predictability using a meteorological model. In addition, the timing of the storm in September facilitates the simulation of the event using a relatively short forecast window, due to the presence of high evapotranspiration which effectively resets soil moisture conditions between flooding periods. While our study is limited to early September 2003, the numerical modeling experiments provide insight into the soil moisture effects on rainfall generation and flood response in a broader region of the southwestern US during the North American monsoon.

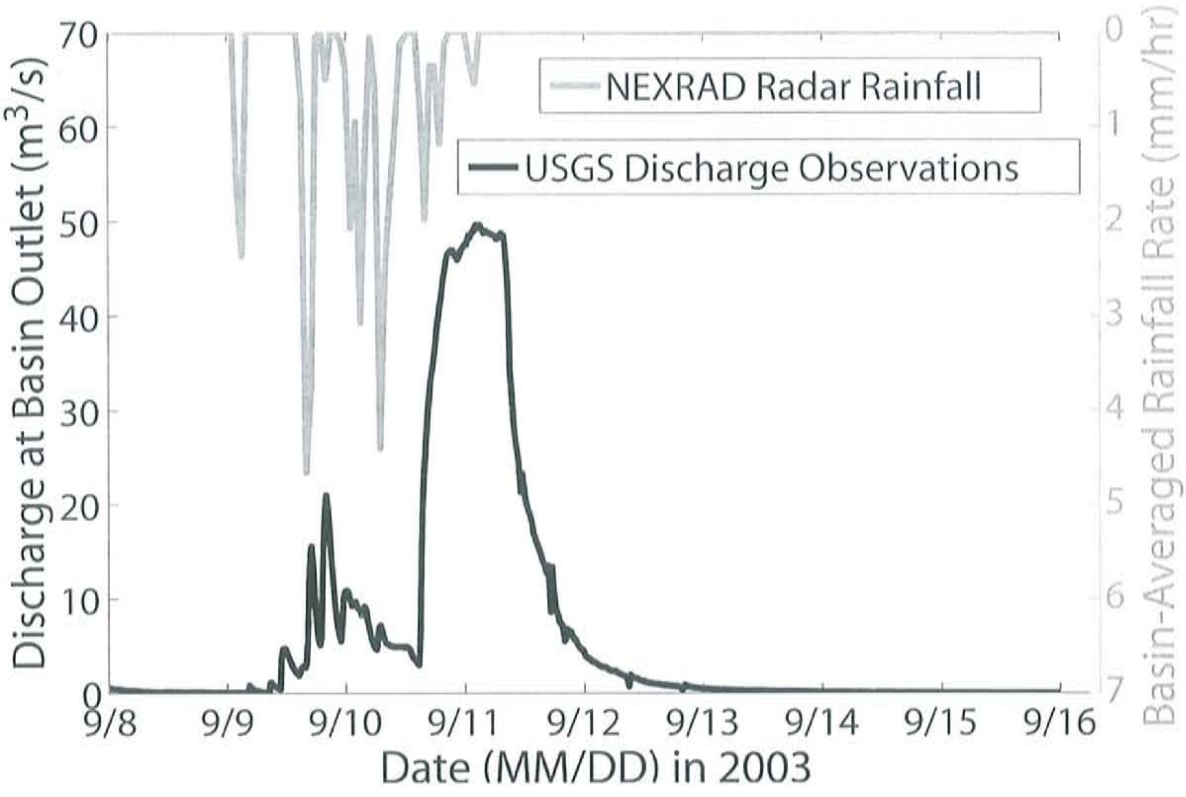


**Figure 2.2.** Rainfall hyetograph (top-axis) and streamflow hydrograph (bottom-axis) in the Upper Río Puerco basin. The radar rainfall hyetograph (mm/hr) represents the basin-averaged rainfall rate obtained from the 4-km NEXRAD (Stage III) hourly data. Discharge hydrograph ($m^3/s$) is shown for the USGS gauging station in the Upper Río Puerco basin above Arroyo Chico Near Guadalupe. Note that the peak discharge is ~50 $m^3/s$. The time to peak was computed based on the rainfall centroid, yielding a value of ~1 day. The runoff ratio was also computed using the flood volume at the gauge ($4.48 \times 10^6$ $m^3$) and the radar rainfall volume ($4.20 \times 10^7$ $m^3$), yielding a value of 0.106 (10.6%) for the flood event (Vivoni et al. 2006).

### 2.2.2 Atmospheric Model: WRF

The atmospheric model utilized for this study is the Weather Research and Forecasting (WRF) Advanced Research WRF (ARW) model. It is a nonhydrostatic, Eulerian mesoscale model (Skamarock et al. 2005) that has been used widely for research and forecasting purposes. For this study, the WRF model Version 2.2 was set up with an outer domain and two nested grids with horizontal spacings of 30, 10, 3.33 km, respectively (Fig. 2.1). Thirty vertical levels were used in the atmospheric columns. The model was driven by North American Regional Reanalysis data (NARR at 32-km resolution) at 3-h intervals for initial and boundary conditions for the outer domain (Mesinger et al. 2006). The following physical parameterizations were utilized in WRF: (1) cloud microphysics from Thompson et al. (2004); (2) longwave radiation based on the Rapid Radiative Transfer Model scheme (Mlawer et al. 1997); (3) shortwave radiation using Dudhia (1989); (4) the planetary boundary layer was based on Mellor-Yamada-Janjic approach (Janjic 2002); (5) the land surface scheme of the Noah land surface model (LSM) was used (Chen and Dudhia 2001); and (6) cumulus parameterization was based on the Kain-Fritsch scheme (Kain and Fritsch 1990). No convective parameterization was used for the finest (3.33-km) domain because deep and shallow convection are explicitly resolved at this resolution. The following paragraph discusses the generation of ensemble rainfall and meteorological fields by using different initial soil moisture conditions.

To generate a set of different initial soil moisture conditions in the WRF model, we multiplied the initial NARR volumetric soil moisture field by a factor, $\alpha$, ranging from 0 to 2.25 (16 different cases). This factor was applied uniformly across

all the soil layers and the three modeling domains. The soil column is represented using four layers (0-10, 10-40, 40-100, 100-200 cm layer thicknesses) and parameterized based on properties inferred from texture classification. The initial soil moisture was scaled by the multiplication factor ($\alpha$) at the beginning of the WRF simulation and was then allowed to evolve in the Noah LSM. Figure 2.3 illustrates the initial soil moisture field ($m^3/m^3$) for the top layer (0 to 10 cm in depth) over the three domains for $\alpha$ = 0.0 and 2.25. Figure 2.4 describes the statistical properties of the initial volumetric soil moisture field ($m^3/m^3$) for the top layer (0 to 10 cm in depth) over the three domains. The spatial field mean and maximum soil moisture increase almost linearly with the soil moisture multiplier ($\alpha$ below 1.5) and then increase in a non-linear fashion when approaching $\alpha$ = 2.25. Note that the standard deviation also increases with the multiplier $\alpha$ for all three domains as soil moisture in some areas approaches the maximum storage capacity equal to the soil porosity. The minimum soil moisture for both domains 1 and 2 remains constant since there are some regions with low porosity soils (approaching zero) which are relatively unaffected by the soil moisture multiplier.

We focused our WRF simulations on a relatively short period (a four-day forecast) with a significant monsoon storm event in the Upper Río Puerco. Our objective in using the model was to reasonably reproduce the sequence of convective cells that led to rainfall in the basin. Simulated rainfall accumulations were compared against weather radar observations (Vivoni et al. 2006) to assess model performance. This comparison provided insight into the proper selection of physical parameterizations, boundary conditions and domain representation for our control run

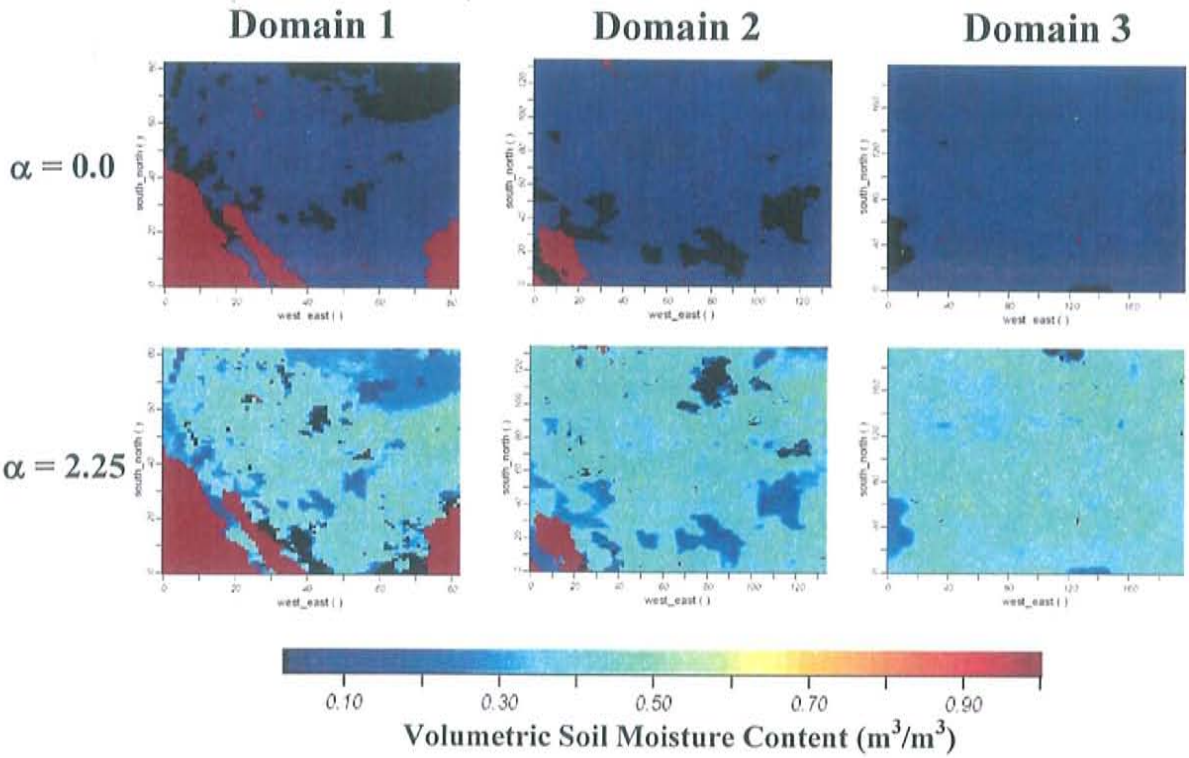


**Figure 2.3.** Effect of the soil moisture multiplier ($\alpha$ = 0.0 and 2.25) on the initial volumetric soil moisture ($m^3/m^3$) in WRF for the top layer (0 to 10 cm in depth) in each domain.

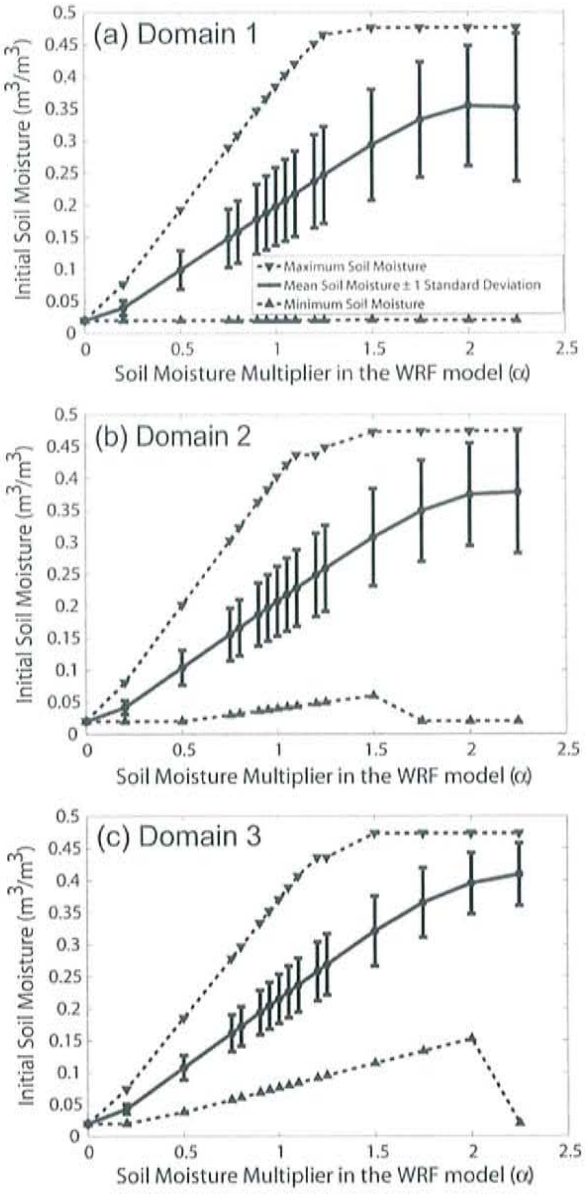


**Figure 2.4.** Effect of the soil moisture multiplier (α, ranging from 0 to 2.25) on the initial soil moisture field in WRF for the top layer (0 to 10 cm in depth) in each domain. The statistical properties of the initial soil moisture for (a) Domain 1, (b) Domain 2, and (c) Domain 3 include the minimum, maximum, and spatial mean volumetric soil moisture ($m^3/m^3$) with ± 1 standard deviation of the spatial soil moisture ($m^3/m^3$).

($\alpha$ = 1) using the WRF model. Variation of the initial soil moisture through the multiplication factor led to fifteen additional WRF simulations (plus one control run) where each case used an identical set of boundary conditions, physical parameterizations and model domain representations. Since the only variation allowed was the vertical soil moisture content in the nested domains, we refer to the simulations as an ensemble generated simply by perturbing initial soil moisture in the NAM region.

### 2.2.3 Distributed Hydrological Model: tRIBS

The TIN-based Real-time Integrated Basin Simulator (tRIBS) is a physically based, fully-distributed hydrological model designed to operate with meteorological forcing from rain gauges, weather radar or numerical weather prediction models (e.g., Ivanov et al. 2004a,b, Vivoni et al. 2005, 2007b). Simulation of the coupled surface and groundwater response to the meteorological forcing is performed by analyzing infiltration fronts, water table fluctuations and lateral moisture fluxes in the vadose and saturated zones depending on vegetation, soil and aquifer properties. Surface runoff is simulated via four different mechanisms: infiltration-excess, saturation-excess, perched return flow and groundwater exfiltration. Routing of surface runoff is performed through hydraulic channel routing and hydrologic overland flow (see Ivanov et al. 2004a). Evapotranspiration is composed of bare soil evaporation, plant transpiration and evaporation of intercepted rainfall, all of which require radiation and energy balance calculations using estimates of the surface meteorological fields.

The tRIBS model domain is a Triangulated Irregular Network derived from a 30 m DEM using a set of techniques described by Vivoni et al. (2004). For the Upper

Río Puerco basin, the TIN domain consists of ~127,000 computational nodes that preserve topographic characteristics in the basin as well as the channel network structure and basin boundary. Approximately 8.9% of the original DEM nodes were preserved through the sampling of points in the TIN model (Wyckoff 2007). A constant area threshold method was employed to classify DEM points as stream cells (Vivoni et al. 2004) and retain these in the model domain. We also delineated a floodplain region from the DEM and represented it within the TIN model using an elevation threshold algorithm of Williams et al. (2000). This allows the relatively flat floodplain topography to be retained at high resolution in the TIN model domain in order to capture near-stream saturation.

The setup of the tRIBS model requires specification of spatially distributed data including topography, soils, vegetation, bedrock depth and the initial groundwater table position. We obtained these datasets from different available geospatial sources, including the National Elevation Dataset (NED), National Resource Conservation Service State Soil Geographic Database (STATSGO), and National Land Cover Data (NLCD). Model parameterization is carried out by specifying soil texture and vegetation properties for each classification derived from available data. To limit the potential for overparameterization, within-class parameter variations are not allowed for soil and vegetation properties. Tables 2.1 and 2.2 present the parameter values for vegetation and soil classifications in the Upper Río Puerco obtained from an extensive model testing exercise for the storm period of interest conducted by Wyckoff (2007). Figure 2.5 presents the spatial distribution of surface soil texture, land cover and initial depth to groundwater used for the URP

| Land Cover Parameters | | | | | | | | | | |
|---|---|---|---|---|---|---|---|---|---|---|
| Land Cover Type | $A$ (%) | $P$ (-) | $S$ (mm) | $K$ (mm/hr) | $g$ ($mm^{-1}$) | $Al$ (-) | $h$ (m) | $K_t$ (-) | $R_s$ (s/m) | $V$ (-) |
| Water | 0.0 | 1.00 | 1.0 | 0.01 | 3.7 | 0.04 | 0.01 | 1.00 | 0.0 | 0.95 |
| Urban | 0.1 | 1.00 | 1.0 | 0.01 | 3.7 | 0.20 | 8.00 | 1.00 | 0.0 | 0.95 |
| Bare Soil | 0.4 | 1.00 | 1.0 | 0.01 | 3.7 | 0.30 | 0.01 | 1.00 | 0.0 | 1.00 |
| Forest | 39.3 | 0.48 | 2.4 | 0.12 | 3.7 | 0.15 | 12.0 | 0.45 | 200 | 0.80 |
| Shrubland | 29.4 | 0.70 | 1.5 | 0.20 | 3.9 | 0.16 | 0.75 | 0.55 | 100 | 0.45 |
| Grassland | 29.2 | 0.85 | 0.8 | 0.10 | 4.2 | 0.13 | 0.18 | 0.70 | 050 | 0.45 |
| Agriculture | 1.6 | 0.75 | 0.8 | 0.10 | 3.6 | 0.20 | 0.40 | 0.65 | 075 | 0.65 |
| Wetlands | 0.0 | 0.90 | 1.0 | 0.10 | 3.6 | 0.14 | 0.50 | 0.50 | 100 | 0.60 |

**Table 2.1** Land cover parameter values for the Upper Río Puerco in the calibrated tRIBS distributed hydrologic model. $A$ is the percentage of basin area of this particular land cover type (%); $P$ is the free throughfall coefficient (-); $S$ is the canopy field capacity (mm); $K$ is the drainage coefficient (mm/hr); $g$ is the drainage exponential parameter ($mm^{-1}$); $Al$ is the albedo (-); $h$ is the vegetation height (m); $K_t$ is the optical transmission coefficient (-); $R_s$ is the canopy-average stomatal resistance (s/m); and $V$ is the vegetation fraction.

| Soil Parameters | | | | | | | | | | |
|---|---|---|---|---|---|---|---|---|---|---|
| Soil Type | $A$ (%) | $K_s$ (mm/hr) | $\Theta_s$ (-) | $\Theta_r$ (-) | $m$ (-) | $\psi_b$ (mm) | $f$ ($mm^{-1}$) | $A_s$ (-) | $A_u$ (-) | $n$ (-) |
| Sandy Loam | 16.4 | 26.8 | 0.412 | 0.041 | 0.378 | -146.2 | 0.00520 | 65 | 140 | 0.453 |
| Loam | 43.3 | 20.50 | 0.434 | 0.030 | 0.252 | -112.2 | 0.00625 | 25 | 125 | 0.463 |
| Unweathered Bedrock | 6.7 | 19.95 | 0.085 | 0.015 | 0.165 | -373.3 | 0.00157 | 25 | 125 | 0.150 |
| Silty Loam | 0.8 | 6.20 | 0.486 | 0.015 | 0.234 | -207.9 | 0.00650 | 65 | 140 | 0.501 |
| Clay Loam | 32.8 | 0.45 | 0.390 | 0.077 | 0.242 | -258.9 | 0.00700 | 50 | 140 | 0.464 |

**Table 2.2** Soil parameter values for the Upper Río Puerco in the calibrated tRIBS distributed hydrologic model. $A$ is the percentage of basin area of this particular soil type (%); $K_s$ is the saturated hydraulic conductivity (mm/hr); $\Theta_s$ is the soil moisture at saturation (-); $\Theta_r$ is the residual soil moisture (-); $m$ is the pore distribution index (-); $\psi_b$ is the air entry bubbling pressure (mm); $f$ is the conductivity decay parameter ($mm^{-1}$); $A_s$ is the saturated anisotropy ratio (-); $A_u$ is the unsaturated anisotropy ratio (-); and $n$ is the porosity (-).

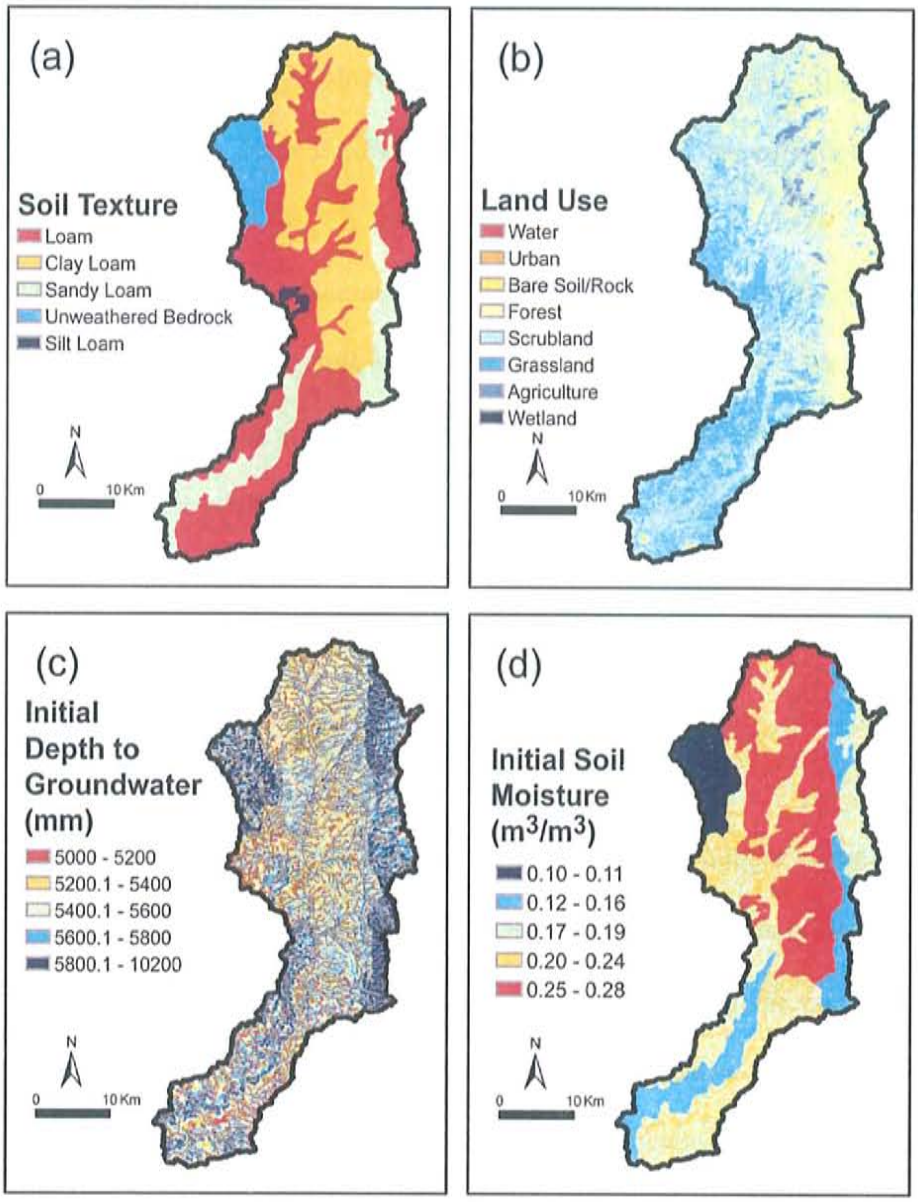


**Figure 2.5.** Spatial distribution of the (a) surface soil texture classification (STATSGO), (b) land use or vegetation type (NLCD), (c) the initial depth to groundwater table (mm) and (d) the initial surface soil moisture ($m^3/m^3$) for the fixed initialization for the Upper Rio Puerco basin as represented in the tRIBS distributed hydrological model.

simulations. tRIBS simulations were conducted for an 8-day period (September 8-16, 2003) with identical hydrological parameterizations except the varying meteorological forcings from the WRF simulations and the specification of initial conditions as described below.

Due to the coupled surface-subsurface nature of the tRIBS model, the depth to the water table controls the soil wetness conditions and defines the initial soil moisture profile (Ivanov et al. 2004a). This relation assumes hydrostatic equilibrium for the vertical distribution of pressure head which corresponds to zero initial flux in the unsaturated zone. The initial groundwater table in a given polygon in a tRIBS application is directly tied to the soil moisture profile by:

$$\theta(n) = \theta_r + (\theta_s - \theta_r)\left[\frac{\psi_b}{n - N_{wt}}\right]^{\lambda(n)} \tag{2}$$

where $\theta_r$ is the residual soil moisture content, $\theta_s$ is the soil moisture at saturation, $\psi_b$ is the air entry bubbling pressure, $n$ is the depth perpendicular to the land surface, $N_{wt}$ is the position of groundwater table, $\lambda(n)$ accounts for changes in pore size with depth (Ivanov et al., 2004a). Because of this relation, we ran a drainage experiment in order to create a reasonable initial groundwater table and associated soil moisture profile for tRIBS initialization (see Vivoni et al. 2005 for another example). In the absence of rainfall and evapotranspiration, this drainage experiment is designed to allow a fully-saturated catchment to drain for a long period of time (~10 years) leading to the readjustment of the subsurface head field in the context of the basin geomorphology (Vivoni et al. 2007c). The baseflow drainage from the basin is subsequently related to the groundwater head fields to derive a groundwater rating curve (e.g. Marani et al. 2001). We performed a first set of ensemble simulations (16 runs, termed as *fixed*

*initial conditions*) using the same soil moisture distribution (see Figure 2.5d) induced by the initial groundwater table from the drainage experiment to match observed baseflow prior to the storm (see Figure 2.5c).

According to equation 2, as the position of groundwater table ($N_{wt}$) increases (i.e., as the groundwater goes deeper), $\theta(n)$ decreases non-linearly. By increasing or decreasing the depth to groundwater, which is derived from the drainage experiment (Figure 2.5c), we generated various initial groundwater fields to match the initial soil moisture conditions between WRF and tRIBS in an aggregated basin-averaged manner. In particular, we manually raised and lowered the groundwater table (Figure 2.5c) uniformly throughout the model domain until a reasonable fit between the two model initializations was found. Because of the variable soil types in the model domain, the soil moisture at individual sites is impacted differently when the uniform increase or decrease in $N_{wt}$ is applied, we increased the number of iterations to fit the initial surface soil moisture between the models. As a result, we adjusted and generated various initial soil moisture conditions in the hydrological model and some example cases were shown in Figure 2.6. We then performed a second set of ensemble tRIBS simulations (13 runs) using the *adjusted initial conditions*. The two sets of ensemble simulations based on fixed and adjusted initial soil moisture conditions were compared to explore the impact of the antecedent soil moisture conditions in the watershed on the hydrologic response. This comparison will also allow determining the need for matching the soil moisture conditions in offline, coupled meteorological and hydrologic models.

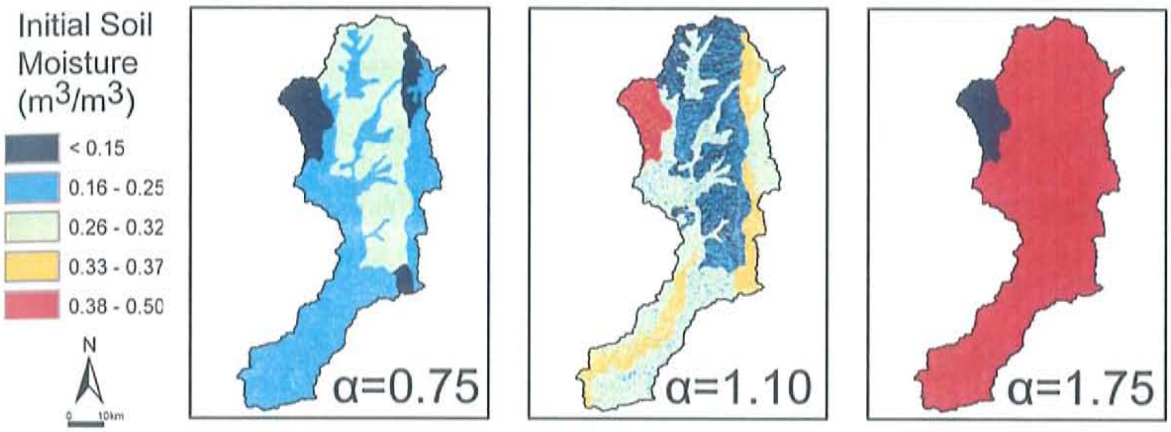


**Figure 2.6.** Spatial distribution of the initial surface soil moisture ($m^3/m^3$) for the adjusted initialization cases for the Upper Rio Puerco basin as represented in the tRIBS distributed hydrological model. Only a selected number of $\alpha$ cases are shown for clarity.

### 2.2.4 Numerical Experiment

A total of six separate meteorological fields from the WRF simulations were used to force the tRIBS hydrological model. To achieve this, hourly meteorological forcing fields including rainfall (mm/hr), atmospheric pressure (mb), air temperature (°C), relative humidity (%), wind speed (m/s) and sky cover were first post-processed from the WRF output at the finest domain (D03) to the grid formatting required for tRIBS. Each of these fields is a standard meteorological output from WRF obtained at or above the land surface at 2 m height with the exception of sky cover. Sky cover ($XC$) ranges from 0 (no clouds) to 10 (overcast) and was computed based on the relative humidity and rainfall occurrence according to Benjamin and Carlson (1986) as:

$$XC = 12.5(3.2RH - 2.4) \quad (1)$$

where $RH$ is the relative humidity (%). Sky cover is set to 10 if rainfall occurs. Sky cover is set to 0 if $RH$ is less than 75%.

The spatial output from WRF (in grid format at 3.3 km resolution) was resampled onto the Upper Río Puerco domain. Model elements in tRIBS are composed of Voronoi polygons (nearest neighborhoods around TIN nodes) which together form a spatially continuous field referred to as the Voronoi Polygon Network (VPN). The gridded WRF output was resampled to the VPN using a nearest neighborhood approach, as performed for gridded NEXRAD radar rainfall data (see Ivanov et al. 2004a). Ensemble members of the hydrological simulations were run for a total of eight days based on the meteorological forcing fields for the two sets of experiments (fixed and adjusted initial conditions). The first four-day period covers

the primary and immediate runoff response to the storm event. To ensure that the streamflow generated during the storm exits through the basin outlet, we extended the hydrologic simulations for an additional four days (from the start of 9/12 to the end of 9/15) using zero rainfall padding and replicating the diurnal meteorological data from the first day of the WRF simulation which exhibited relatively clear conditions.

## 2.3 Results and Discussion

### 2.3.1 Effect of initial soil moisture on basin-scale rainfall properties

We evaluated the monsoon storm meteorological fields over the four-day WRF simulation period to understand the differences in basin-scale rainfall among the sixteen cases with different initial soil moisture conditions ($\alpha$ ranging from 0 to 2.25). Our analysis focuses on rainfall forcing and other meteorological fields at the scale of the hydrological basin. We do not attempt here to provide a detailed assessment of the synoptic storm patterns or dynamical mechanisms leading to rainfall, as these are beyond the scope of our current study. Instead, we highlight those meteorological model results most relevant to forcing the hydrological simulations used to generate streamflow forecasts with extended lead times. This effort takes advantage of the forecast lead times of several days available from numerical weather prediction models to provide long-lead time flood forecasts (e.g., Yates et al. 2000; Westrick and Mass, 2001).

To gain confidence in the meteorological simulation, we first compared the spatial distribution of basin rainfall from the NEXRAD Stage III product (4-km, 1-hr resolutions, Xie et al. 2005) to the WRF control simulation ($\alpha$ = 1, 3.3-km, 1-hr resolutions). Figure 2.7a presents the spatial map of total rainfall accumulation over

the four-day simulation period (September 8-12, 2003). Note that the rainfall ranges of the WRF control run (15 to 82 mm) and NEXRAD (14 to 63 mm) are quite similar. Nevertheless, there are clear differences in the spatial pattern of total rainfall accumulation. The WRF simulation is organized according to the basin topography with higher values along the Nacimiento Mountains and lower rainfall amounts in the desert lowlands. NEXRAD, on the other hand, exhibits lower than expected rainfall amounts along the mountain front potentially due to beam blockage effects from the Albuquerque NWS radar site, located to the southeast of the basin. The agreement between the two estimates is improved in the desert lowlands near the basin outlet.

Figure 2.7b also compares the hourly basin-averaged rainfall for the NEXRAD estimates and WRF simulations. Note that the rainfall timing is similar during the peak storm activity on September 10, 2003, although the rainfall peak magnitudes for NEXRAD are larger than the WRF simulation by a factor of 1.5. Furthermore, the WRF simulation reproduces the distinct storm cells traversing the basin from west to east with approximately the correct timings and interstorm spacing. Based on the similarities in rainfall accumulation and timing, the WRF control simulation ($\alpha = 1$) is considered to perform reasonably well for the storm period of interest. As a result, the WRF physical parameterizations of the control run were adopted for the ensemble simulations.

Figure 2.8 presents the mean areal rainfall over the Upper Río Puerco as obtained from the different soil moisture initializations. The basin-averaged rainfall rate is used as a first-order metric to compare the WRF simulations and diagnose the impact of different initial soil moisture conditions. Note that the basin-averaged

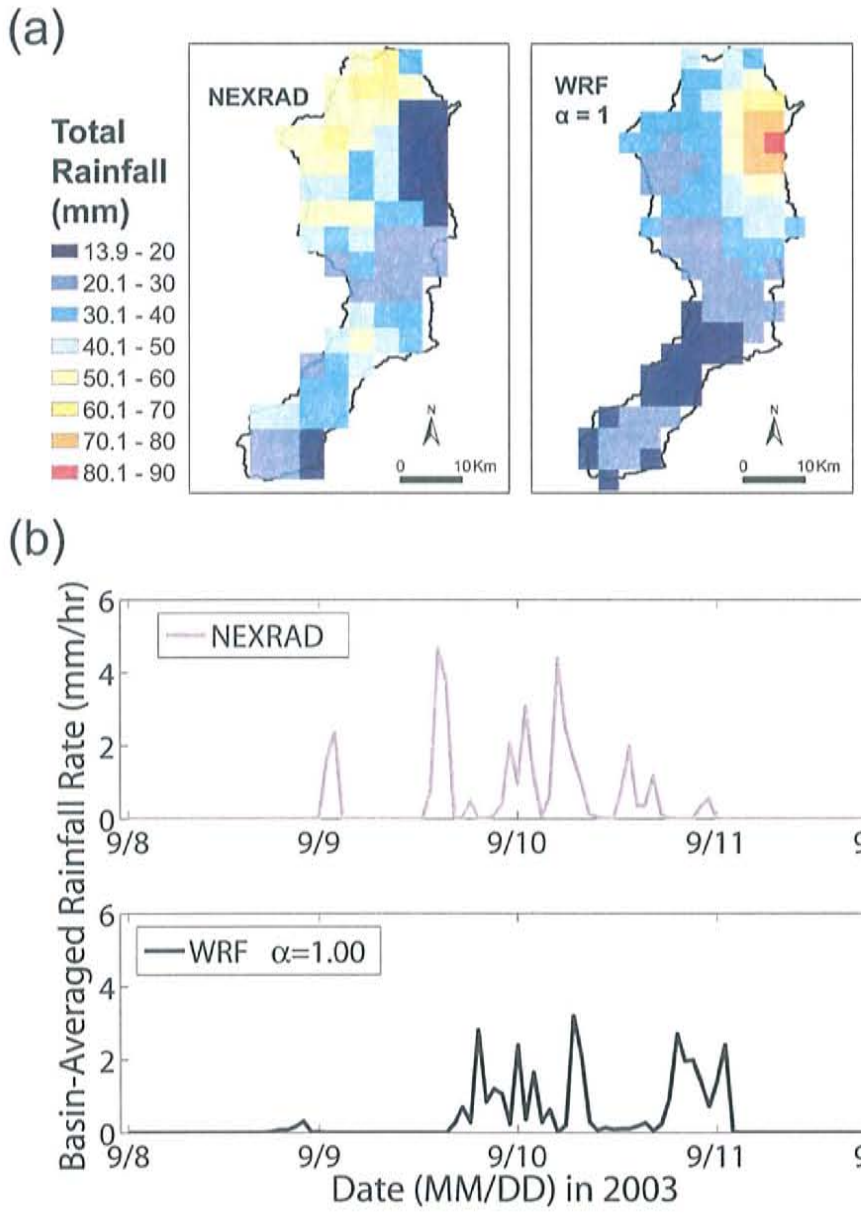


**Figure 2.7.** Rainfall comparison between NEXRAD Stage III product (4-km, 1-hr resolutions) and WRF control simulation ($\alpha$=1, 3.3-km, 1-hr resolutions) for (a) the spatial distribution of total storm rainfall (mm), and (b) the temporal distribution of basin-averaged rainfall rate (mm/hr).

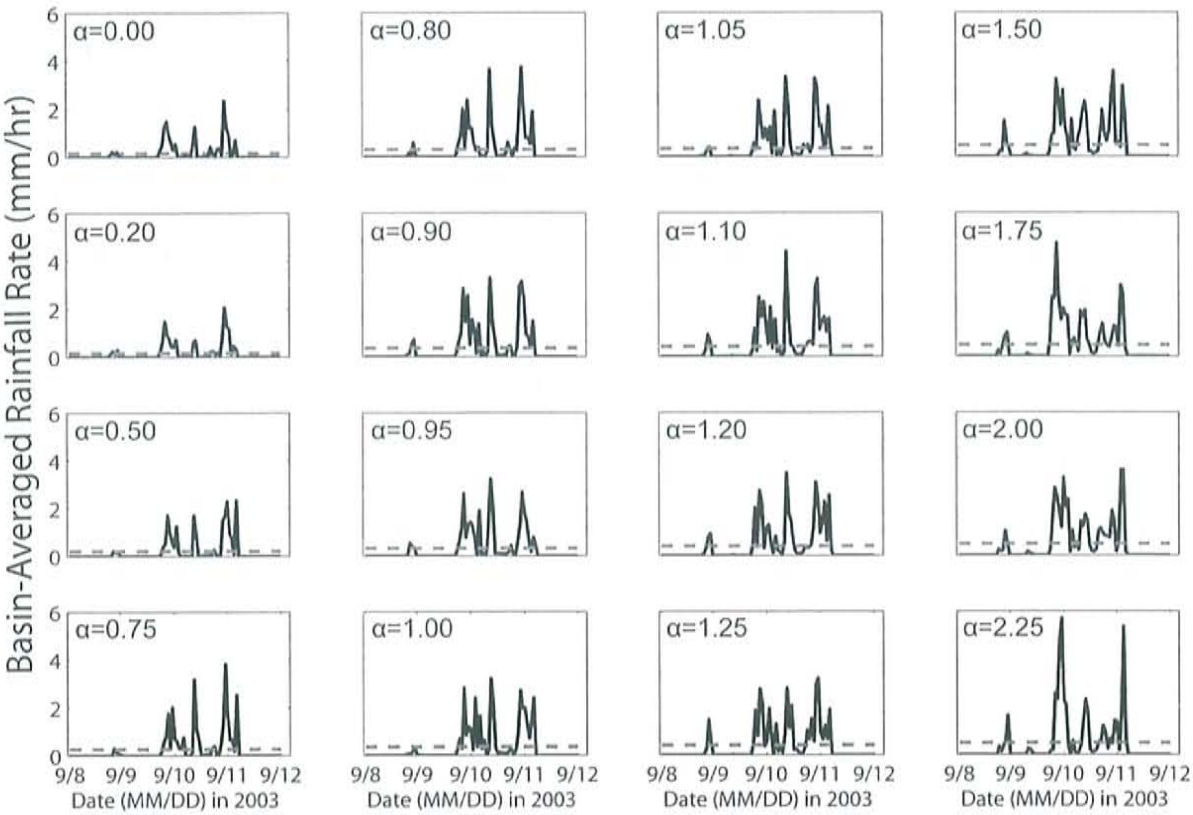


**Figure 2.8.** Comparison of the hourly basin-averaged rainfall rate (mm/hr) for different initial soil moisture conditions ($\alpha$ = 0 to 2.25) in the WRF model over the Upper Río Puerco. The horizontal dashed lines represent the temporal mean of the basin-averaged rainfall. Note that increasing $\alpha$ occurs along columns from top to bottom.

rainfall magnitude increases considerably with the initial soil moisture content, with peaks of ~2 mm/hr for $\alpha = 0$ and ~6 mm/hr for $\alpha = 2.25$, across the different storm cells traversing the basin. This suggests that regional soil moisture directly influences the rainfall generation process and its intensification for this large storm event. As a consequence, the temporal mean of the basin-averaged rainfall also increases with the initial soil moisture. In general, the timing of rainfall peaks for individual storm cells are coincident for the simulations, suggesting a stronger soil moisture control on rainfall intensity as compared to rainfall timing.

To complement this analysis, Figure 2.9 presents the temporal variations in the rainfall coverage ($A_R$) for the Upper Río Puerco for the different initial soil moisture conditions ($\alpha = 0$ to 2.25). This spatial metric identifies the percentage of the basin area that experiences rainfall greater than zero ($R > 0$). Relatively longer and more pronounced rainfall coverages in the basin are associated with higher initial soil moisture. Note also that the temporal mean rainfall coverage increases slightly with the soil moisture content. Clearly, the first storm cell in the basin on September 9, 2003, was of limited spatial extent, while the primary storm cells on September 10-11, 2003, had partial to full coverage in the basin, for all initial conditions. These findings suggest that increased regional soil moisture promotes more widespread storms which typically have greater temporal durations. Note that the percentage of time with full rainfall coverage in the basin ($A_R = 100\%$) also increases with the initial soil moisture. This metric has important implications for the solar radiation at the land surface and thus the evapotranspiration response to the storm event.

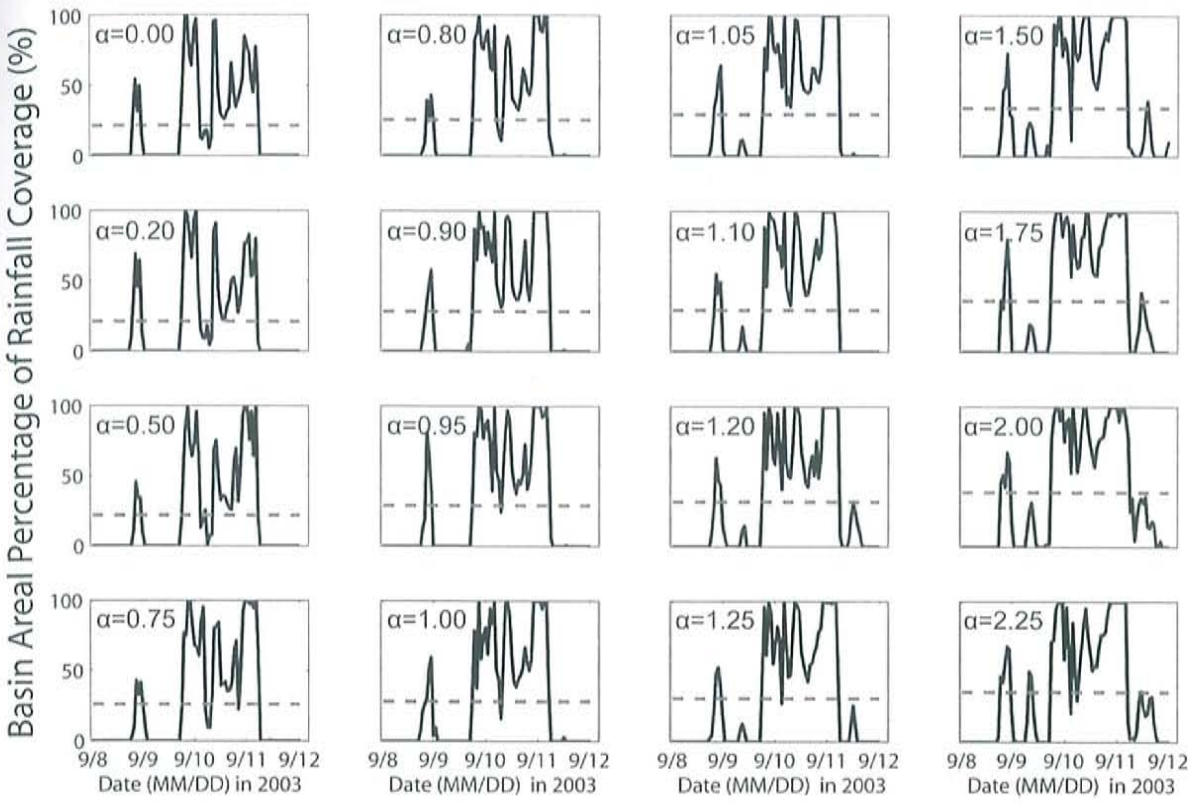


**Figure 2.9.** Comparison of the basin rainfall coverage ($A_R$ in %) depicted as the percentage of total basin area with rainfall greater than zero. The horizontal dashed lines represent the temporal mean of the basin rainfall coverage.

To further investigate the impact of soil moisture on basin-scale rainfall patterns, we analyzed the spatial distribution of the meteorological fields. Figure 2.10 presents the spatial distribution of the total basin rainfall accumulation over the storm period (mm) for different initial soil moisture conditions (increasing $\alpha$). Higher rainfall accumulation in most pixels (3.3 km by 3.3 km) is associated with higher initial soil moisture. Furthermore, a noticeable increase in the areal extent of the storm maximum is observed over the high terrain of the Nacimiento Mountains. This is consistent with the more pronounced rainfall coverage previously identified and suggests an important interaction between initial soil moisture and orographically-induced rainfall. This is a characteristic of the WRF model. Note that the spatial location of maximum rainfall accumulation tends to vary among the simulations, but remains in the general vicinity of the northeast portion of the basin. Furthermore, the rainfall accumulations in the northwestern section of the basin match the unobstructed NEXRAD observations quite well, for $\alpha = 1.5$ or higher.

Rainfall field statistics in the Upper Río Puerco were also computed as a function of initial soil moisture. Figure 2.11a presents the variation of the basin total rainfall volume ($m^3$). Clearly, the rainfall volume increases with increasing $\alpha$, suggesting a positive relation between rainfall generation and initial soil moisture. Note, however, that limited increases in rainfall volume occur for $\alpha$ greater than 1.5, or between $\alpha = 0$ and $\alpha = 0.25$. This indicates that, for this particular event, initial soil moisture linearly controls rainfall volume over the range $\alpha = 0.25$ to 1.5. Further gains in initial soil moisture beyond $\alpha = 1.5$ do not contribute to enhancing the rainfall generation process. Figure 2.11b and 2.11c present the maxima of the basin-

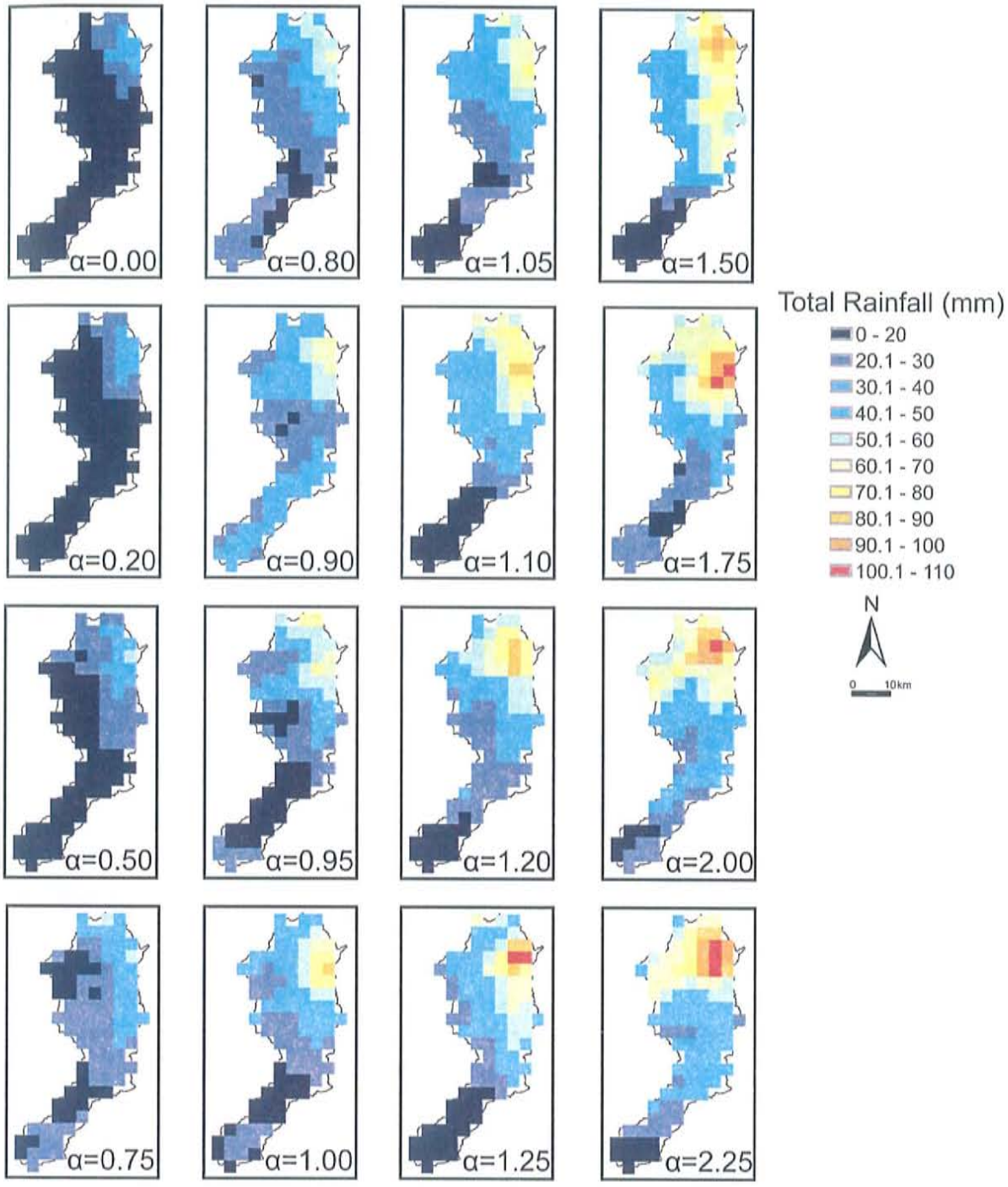


**Figure 2.10.** Comparison of the spatial distributions of total rainfall accumulation during the storm period (mm), September 8-12, 2003, for the different initial soil moisture conditions ($\alpha$).

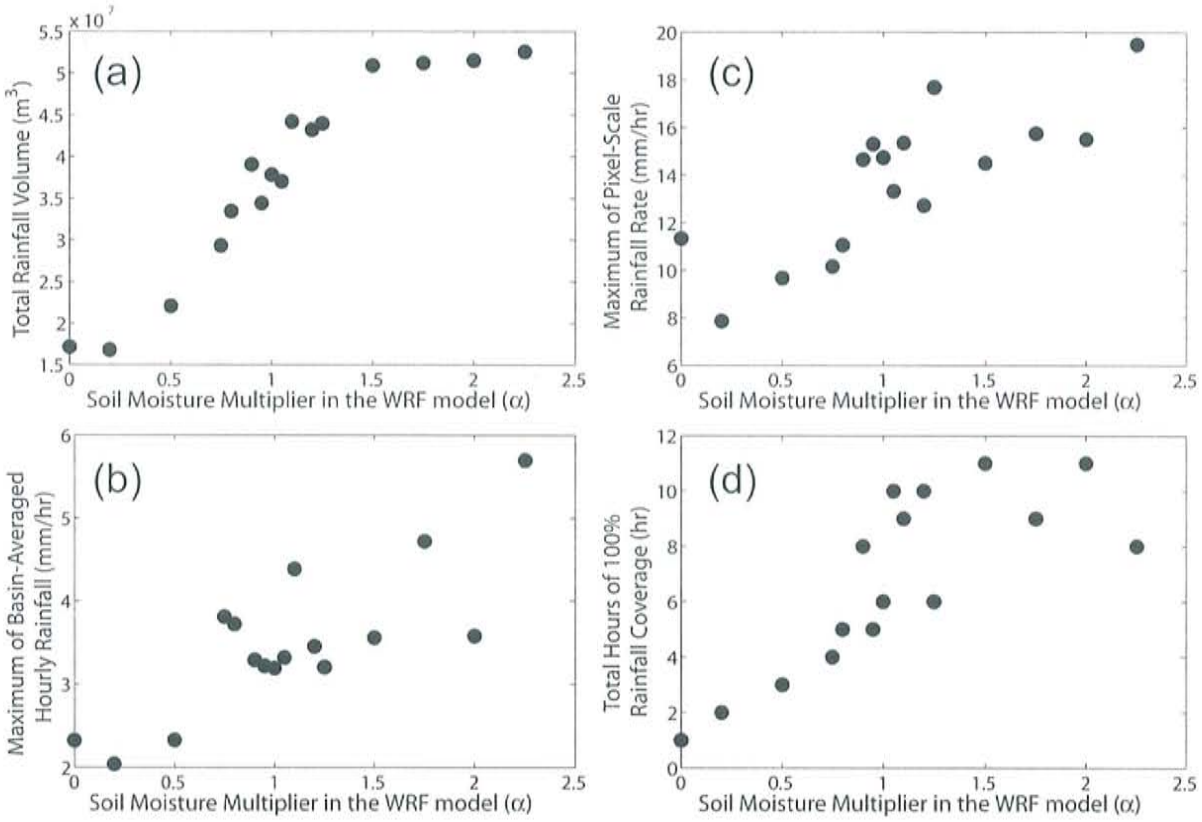


**Figure 2.11.** Impact of the initial soil moisture multiplier on rainfall field statistics over the Upper Río Puerco. (a) Total rainfall volume ($m^3$). (b) Maximum of basin-averaged hourly rainfall (mm/hr). (c) Maximum of pixel-scale rainfall rate (mm/hr). (d) Total length of time with rainfall coverage at 100% of basin area (hr).

averaged and pixel-scale hourly rainfall during the simulation period. These statistics indicate that increases in initial soil moisture lead to increases in the maximum rainfall intensity at both point and regional scales. This sensitivity confirms the variation of the basin rainfall fields observed in Figure 2.10 and also reveals that maximum rainfall rates can vary considerably between simulations while exhibiting an overall increase in intensity with $\alpha$. Variations around the linear trend are due to the complex nature of rainfall generation process and its sensitivity to initial conditions. Figure 2.11d shows the total length (hr) of full rainfall coverage in the basin to support the previous discussion. This metric highlights the relatively longer rainfall coverages simulated for the monsoon storm for the cases of wetter initial conditions.

In summary, the rainfall analysis consistently indicates the enhancement effect of initial soil moisture condition on rainfall properties (i.e., duration, intensity and spatial coverage). Further increases of soil moisture beyond $\alpha = 2.25$ did not enhance rainfall generation (not shown). The observed threshold behavior in the soil moisture control on rainfall beyond approximately $\alpha = 1.5$ is likely a result of other limitations of the convection processes. For example, Kim and Wang (2007a) found that increases of soil moisture beyond a certain level no longer promoted continued evapotransipiration due to radiation limitations. In our simulations, the rainfall generation process can be limited by available energy or synoptic scale factors which would prevent further increases in rainfall beyond a particular soil moisture amount. Note that the threshold does not occur for fully wet soils but rather at soil moisture values of ~0.3 $m^3/m^3$ ($\alpha = 1.5$; see Figure 2.4). This indicates that soil moisture

conditions within plausible ranges in the region can have impact on rainfall generation. Moreover, similarities in storm timing suggests that the major differences among the simulations are in the rainfall intensity, location and coverage.

### 2.3.2 Effect of rainfall forcing on hydrologic response under fixed initializations

We utilized the WRF simulations with the different initial soil moisture as forcing to the distributed hydrological model. In this section, we analyze results for the tRIBS simulations with fixed initial conditions. We first inspect the cumulative rainfall volume, basin-averaged surface soil moisture and the cumulative outlet discharge (Figure 2.12). As discussed previously, an increase is observed in storm rainfall accumulation with the initial soil moisture. Cumulative rainfall across each simulation shares similar temporal patterns confirming comparable storm timings. Nevertheless, the spread of the cumulative rainfall is large among the simulations, indicating that perturbations in the initial soil moisture have a significant effect. The pattern of NEXRAD cumulative rainfall is different from that of the ensemble mean due to the differences in spatiotemporal characteristics between the NEXRAD and WRF simulated rainfall. These differences lead to the different patterns of basin-averaged soil moisture between the NEXRAD and the ensemble mean (Figure 2.12b). Interestingly, the basin-averaged soil moisture at the surface differs in both temporal distribution and magnitude with a general increase in soil moisture for higher rainfall (Figure 2.12b). However, some cases below a low $\alpha$ threshold ($\alpha = 0$ and 0.2) or high $\alpha$ high threshold ($\alpha > 1.5$) share respectively similar soil moisture patterns with a small differences in magnitude. This is due to relatively minor differences in rainfall forcing among these cases and the fixed initial conditions assumed in the hydrological

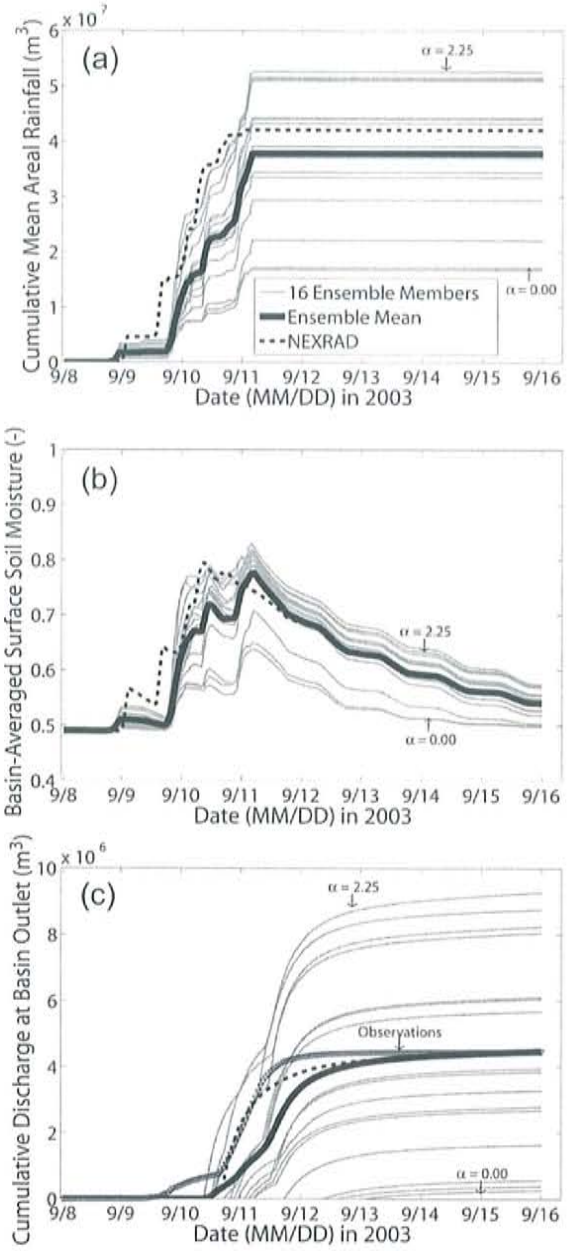


**Figure 2.12.** Comparison of basin hydrologic response for simulations with different WRF initial soil moisture ($\alpha$ = 0 to 2.25) and fixed initial soil moisture conditions in tRIBS. (a) Cumulative basin-averaged rainfall volume ($m^3$). (b) Basin-averaged mean surface soil moisture (in top 10 cm), expressed as relative saturation ($s = \theta / n$); $\theta$ is the volumetric soil moisture content ($m^3/m^3$) and $n$ is the soil porosity. (c) Cumulative discharge ($m^3$) at the Upper Río Puerco basin outlet. Note that the USGS streamflow observations, the NEXRAD forcing and its associated hydrological response based on model simulations is included for comparison purposes. The ensemble mean over the 16 different cases is shown with the solid black lines.

model. Note that the range of final soil moisture among the cases at the end of the simulation is relatively small ($s$ = 0.5 to 0.6) compared to the range during the peak storm activity ($s$ = 0.625 to 0.825). This suggests that the dry-down after the storm event homogenizes soil moisture characteristics across the different cases with fixed initial conditions imposed in the hydrologic model.

Figure 2.12c presents the cumulative discharge at the basin outlet resulting from the storm event. Note that the relatively constant cumulative discharge at the end of simulations indicates that most of the flooding has exited through the basin outlet by this time. Cumulative discharge is generally larger for cases of higher initial soil moisture (~9 x $10^6$ $m^3$). Clearly, the difference in rainfall amount propagates to both the soil moisture and discharge predictions. Because the cumulative rainfall of NEXRAD is higher than that of the ensemble mean, prior to 9/13, the cumulative discharge of NEXRAD is higher than that of the ensemble mean. Note also USGS streamflow observations are close to NEXRAD driven streamflow and the ensemble mean in terms of their magnitudes of cumulative discharge at the end of simulations. Nevertheless, compared to the basin-averaged soil moisture, runoff production and streamflow discharge are more sensitive to differences in the rainfall duration, timing and intensity. In particular, the variation of pixel-scale rainfall intensity leads to differences in infiltration-excess runoff in the hydrologic simulations. Infiltration-excess runoff occurs during unsaturated conditions, when the rainfall rate is greater than the vertical redistribution of water near the soil surface. Rainfall exceeding the infiltration capacity of the soil (see Table 2.2) results in runoff production and streamflow generation. For low $\alpha$, most of the rainfall infiltrates into the soil, leaving

a small proportion available for runoff, whereas for high $\alpha$, a larger fraction of the rainfall exceeds the soil infiltration capacity and produces runoff. In the model parameterization for the URP basin, infiltration-excess runoff is the primary mechanism for overland flow generation given the soil properties, antecedent wetness and rainfall in the semiarid environment, consistent with other studies (e.g., Beven 2002, Castillo et al. 2003, Wyckoff 2007).

To examine the spatial distribution of the runoff generation, Figure 2.13 presents the spatial maps of the percent of time with infiltration-excess runoff occurrence (%) during September 8-16, 2003, for the fixed initial soil moisture conditions. Higher percentages of time with infiltration-excess are associated with higher initial soil moisture due to the greater rainfall intensity simulated at the pixel and basin-scales. Note that the locus of runoff production is in the north central portion of the basin, a region characterized by clay loam soils (see Figure 2.5a). Clearly, the spatial distribution of infiltration excess runoff matches well with the distribution of soil texture. In particular, there is approximately no infiltration-excess runoff on those regions of high saturated hydraulic conductivity (i.e., loam and sandy loam) suggesting the infiltration-excess runoff is driven by the soil properties. Because the high conductivity soils have a higher infiltration capacity less surface runoff will be generated. In the region dominated by clay loam which has a very low saturated conductivity (e.g., 0.45 mm/hr), the percent time with infiltration-excess runoff increases in areas with increasing rainfall intensity (see Figure 2.10) highlighting the impacts of both rainfall intensity and soil properties on the infiltration-excess runoff generation process. Furthermore, while the highest rainfall

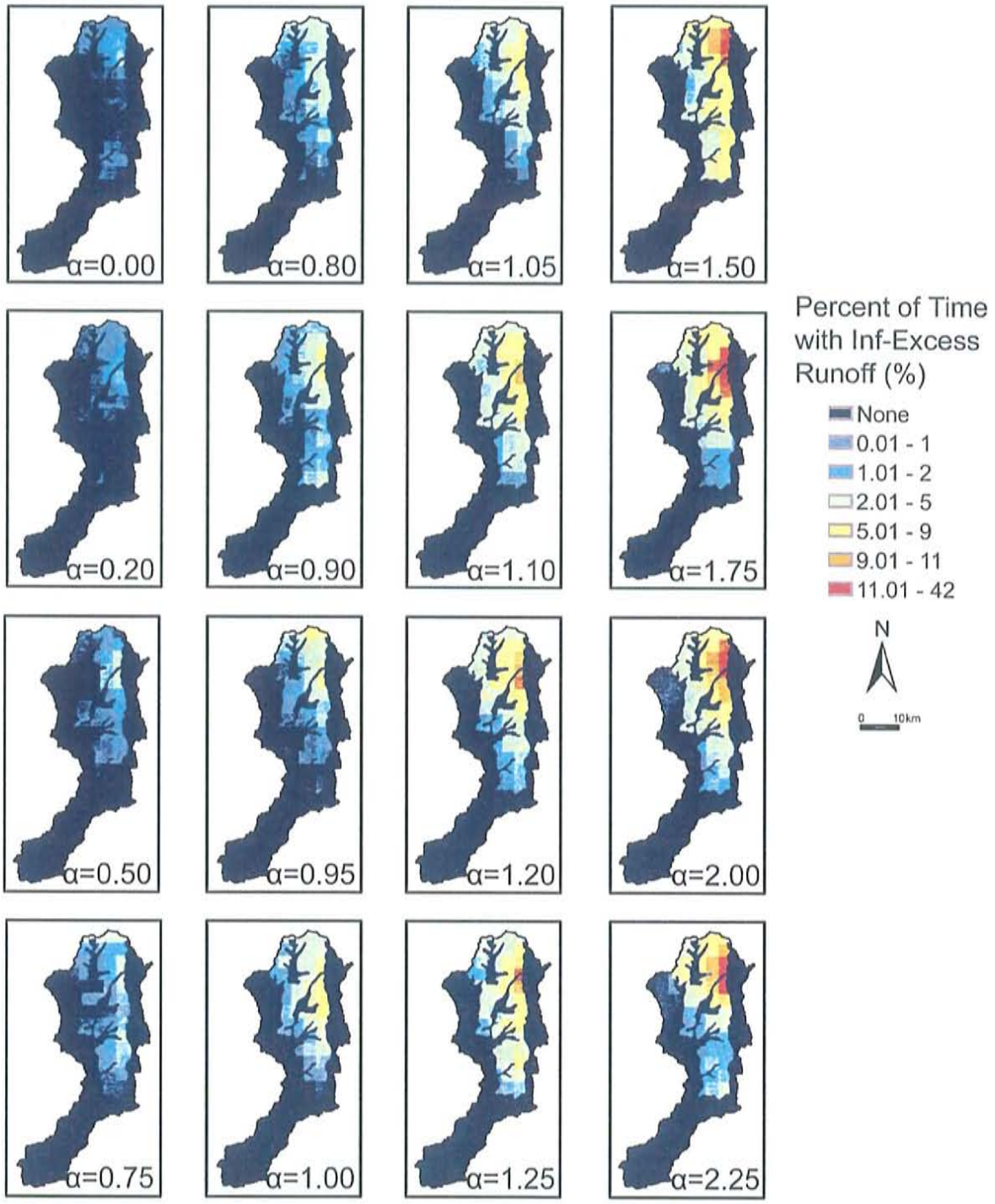


**Figure 2.13.** Spatial distributions of the percent of time with infiltration-excess runoff occurrence (%) during September 8-16, 2003, for the fixed initial soil moisture conditions.

intensities occurred along the Nacimiento Mountains, these generated reduced runoff due to canopy coverage, permeable soils and relatively deep initial groundwater table positions. Note that the runoff production within the clay loam region exhibits the spatial pattern of the WRF rainfall as modified by underlying differences in land cover topography and initial soil moisture.

In summary, the variation in rainfall volume induced by the initial soil moisture in WRF propagates to both the soil moisture and discharge predictions in the tRIBS model. Under these hydrologic simulations with fixed initializations, infiltration-excess runoff is the primary runoff generation mechanism in the URP basin. The spatial distribution of infiltration-excess runoff is governed primarily by both rainfall and soil properties. Soil types with high saturated hydraulic conductivity are less sensitive to changes in rainfall as compared to low conductivity soils. As a result, soils with low permeability are primarily responsible for the occurrence of infiltration-excess runoff induced by rainfall changes among the ensemble members with fixed initializations.

### 2.3.3 Effect of rainfall forcing on hydrologic response under adjusted initializations

To study the effect of the initial soil moisture condition in the hydrologic model response, we attempted to match the basin-averaged surface soil moisture specified in the tRIBS and WRF models. Because the soil moisture profile is tied to the groundwater table position in tRIBS (Ivanov et al. 2004a), we varied the reference initial groundwater table derived from the drainage experiment (Figure 2.5c). This was achieved by uniformly increasing or decreasing the spatial field until a matching

surface soil moisture was achieved for each pair of WRF-tRIBS simulation. This procedure permits a more realistic representation of the effect of initial soil moisture conditions in the hydrologic response, while preserving the spatial soil moisture patterns inherent in each model. As shown in Table 2.3, we were able to match thirteen of the simulation cases (except the drier cases, $\alpha$ = 0, 0.2 and 0.5). Some examples of adjusted soil moisture initializations were shown in Figure 2.6. For the three dry cases, the initial soil moisture in tRIBS could not be decreased significantly under the current physical parameterization. As a result, we will focus attention on an ensemble of the 13 tRIBS simulations obtained under adjusted conditions.

Figure 2.14 shows the cumulative rainfall, surface soil moisture and cumulative discharge across each simulation for the adjusted initializations. Note that the different cases commence with a different initial soil moisture in tRIBS equivalent to the initializations ($\alpha$) specified in WRF (Figure 2.14b). The soil moisture pattern of NEXRAD remains the same as in Figure 2.12b due to using the fixed initial groundwater table input (shown in Figure 2.5c) and NEXRAD rainfall forcing. Note that the ensemble mean of soil moisture is greater than NEXRAD because of the influences of the ensemble members with higher initial soil moisture conditions. Three ensemble members ($\alpha$ = 1.75, 2.00 and 2.25) have the same soil moisture ($s$ = 1) as these are initially saturated. The basin-averaged soil moisture patterns differ in temporal distribution and magnitude among the cases, indicating a general increase for higher $\alpha$. Some cases with low $\alpha$ (e.g., $\alpha$ = 0.75 and 0.85) have a similar soil moisture pattern due to small differences in rainfall forcing and nearly equal initial conditions in the hydrological model. By design, the basin-averaged soil moisture

| $\alpha$ | Mean Depth to Initial Grounwater Table (mm) | Standard Deviation (mm) | Basin-Averaged Volumetric Soil Moisture ($m^3/m^3$) | Standard Deviation ($m^3/m^3$) |
|---|---|---|---|---|
| 0.75 | 7522.3 | 293.7 | 0.20 | 0.06 |
| 0.80 | 5522.3 | 293.7 | 0.21 | 0.05 |
| 0.90 | 2522.3 | 293.7 | 0.24 | 0.06 |
| 0.95 | 1772.3 | 293.7 | 0.26 | 0.06 |
| 1.00 | 1522.3 | 293.7 | 0.27 | 0.06 |
| 1.05 | 1322.3 | 293.7 | 0.28 | 0.06 |
| 1.10 | 1022.3 | 293.7 | 0.30 | 0.07 |
| 1.20 | 772.3 | 293.7 | 0.32 | 0.08 |
| 1.25 | 622.3 | 293.7 | 0.34 | 0.08 |
| 1.50 | 221.8 | 233.1 | 0.40 | 0.09 |
| 1.75 | 0.0 | 2.6 | 0.44 | 0.07 |
| 2.00 | 0.0 | 2.6 | 0.44 | 0.07 |
| 2.25 | 0.0 | 2.6 | 0.44 | 0.07 |

**Table 2.3.** The mean and standard deviation of the depth to initial groundwater table (mm) and basin-averaged volumetric soil moisture (m3/m3) for each adjusted initialization ($\alpha$).

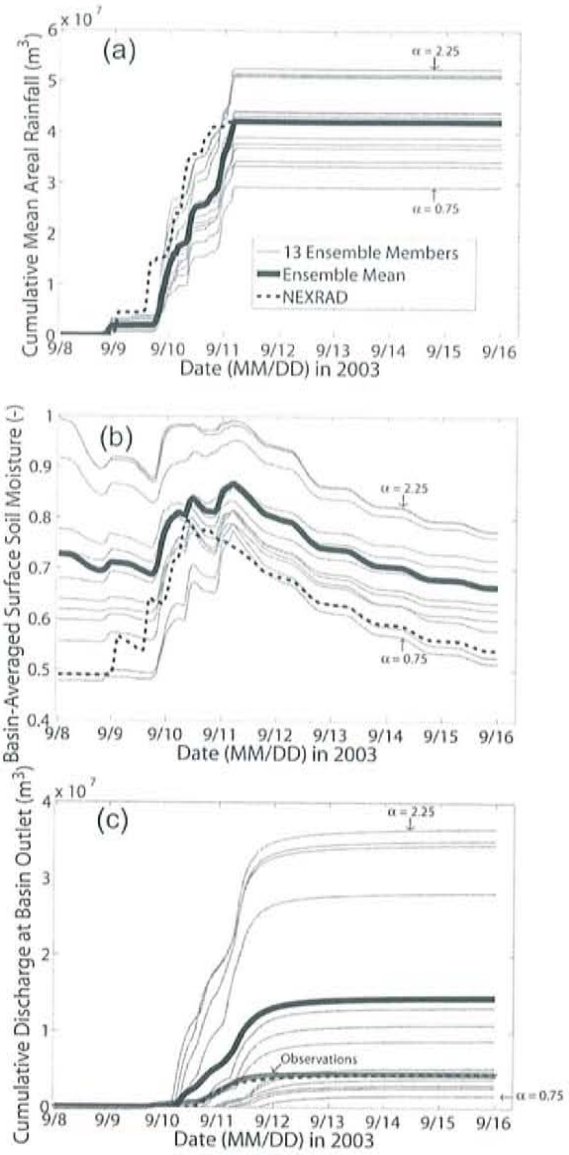


**Figure 2.14.** Comparison of basin hydrologic response for simulations with adjusted initial soil moisture conditions in tRIBS and WRF ($\alpha$ = 0.75 to 2.25). (a) Cumulative basin-averaged rainfall volume ($m^3$). (b) Basin-averaged mean surface soil moisture (in top 10 cm), expressed as relative saturation ($s = \theta / n$); $\theta$ is the volumetric soil moisture content ($m^3/m^3$) and $n$ is the soil porosity. (c) Cumulative discharge ($m^3$) at the Upper Río Puerco basin outlet.

varies among the different cases at the beginning of the simulation ($s$ = 0.48 to 1). Note that soil moisture traces converge during the peak storm period on September 10, 2003. The range of final soil moisture among the different cases is larger ($s$ = 0.53 to 0.77), than for the case of fixed initialization (see Figure 2.12b), suggesting that the effect of the initial condition is important throughout the simulation period. Interestingly, the soil moisture in the last four days (September 12 to 16, 2003) decreases continuously as the surface dries through evapotranspiration and the simulations once again diverge. Given the identical atmospheric forcing during the period, this divergence is due primarily to the differences in drainage for different soil moisture contents. Soil moisture also impacts evapotranspiration rates, but this in general would lead to a convergence of simulations during the interstorm period.

Figure 2.14c presents the cumulative discharge at the basin outlet over the 8-day simulation period. Similar to the set of fixed initialization runs, the cumulative discharge generally increases with the initial soil moisture ($\alpha$) in WRF. Note that the ensemble mean of discharge is higher than NEXRAD due to the influence of high initial soil moisture conditions. A major difference between the two scenarios is the magnitude of the discharge response. The adjusted initial conditions increase the initial soil moisture in tRIBS and lead to a more pronounced streamflow. Note also the ensemble mean discharge are significantly higher than USGS streamflow observations at the end of simulations. The range of the cumulative discharge is much larger (~3.5 x $10^7$ $m^3$) for the adjusted initializations as compared to the fixed initialization cases (~9 x $10^6$ $m^3$). This suggests that appropriately matching the soil moisture initialization of offline coupled models has a significant effect on soil

moisture and runoff predictions. It is important to understand the physical reasons in the hydrological model for the observed increase in streamflow discharge. Recall that the cases with fixed initialization produce infiltration-excess runoff exclusively. In the following, we explore if the increase in discharge can be attributed to changes in the runoff production mechanisms.

Figure 2.15 presents the spatial distributions of the percent of time with saturation excess runoff occurrence (%) for the adjusted soil moisture cases during the 8-day period (September 8-16, 2003). Saturation-excess runoff occurs the soil is completely saturated and the soil can no longer store additional moisture. Any rainfall fallen on the saturated soil becomes saturation-excess runoff. For the most dry cases $\alpha$ = 0.75 to 0.90, there is no occurrence of saturation-excess runoff because infiltration-excess is the primary runoff production mechanism. Starting from $\alpha$ = 0.95, however, the percent time of saturation-excess runoff gradually increases with the higher rainfall induced by the wetter initial conditions. This suggests saturation-excess runoff becomes a prominent mechanism possibly overtaking infiltration-excess runoff, in particular for the saturated initial conditions ($\alpha$ = 1.75). As the surface approaches saturation, there is limited storage capacity for rainfall to infiltrate into the land surface and runoff is generated through the saturation-excess mechanism. In contrast to Figure 2.13 of the fixed initialization cases, the spatial distribution of saturation-excess runoff for $\alpha$ = 1.50 to 2.25 does not match the soil texture field since the surface saturation reduces the role of soil hydraulic properties in runoff production. As a result, saturation-excess runoff is primarily sensitive to rainfall conditions for the wet initial soil moisture ($\alpha$ = 1.50 to 2.25). In particular, the

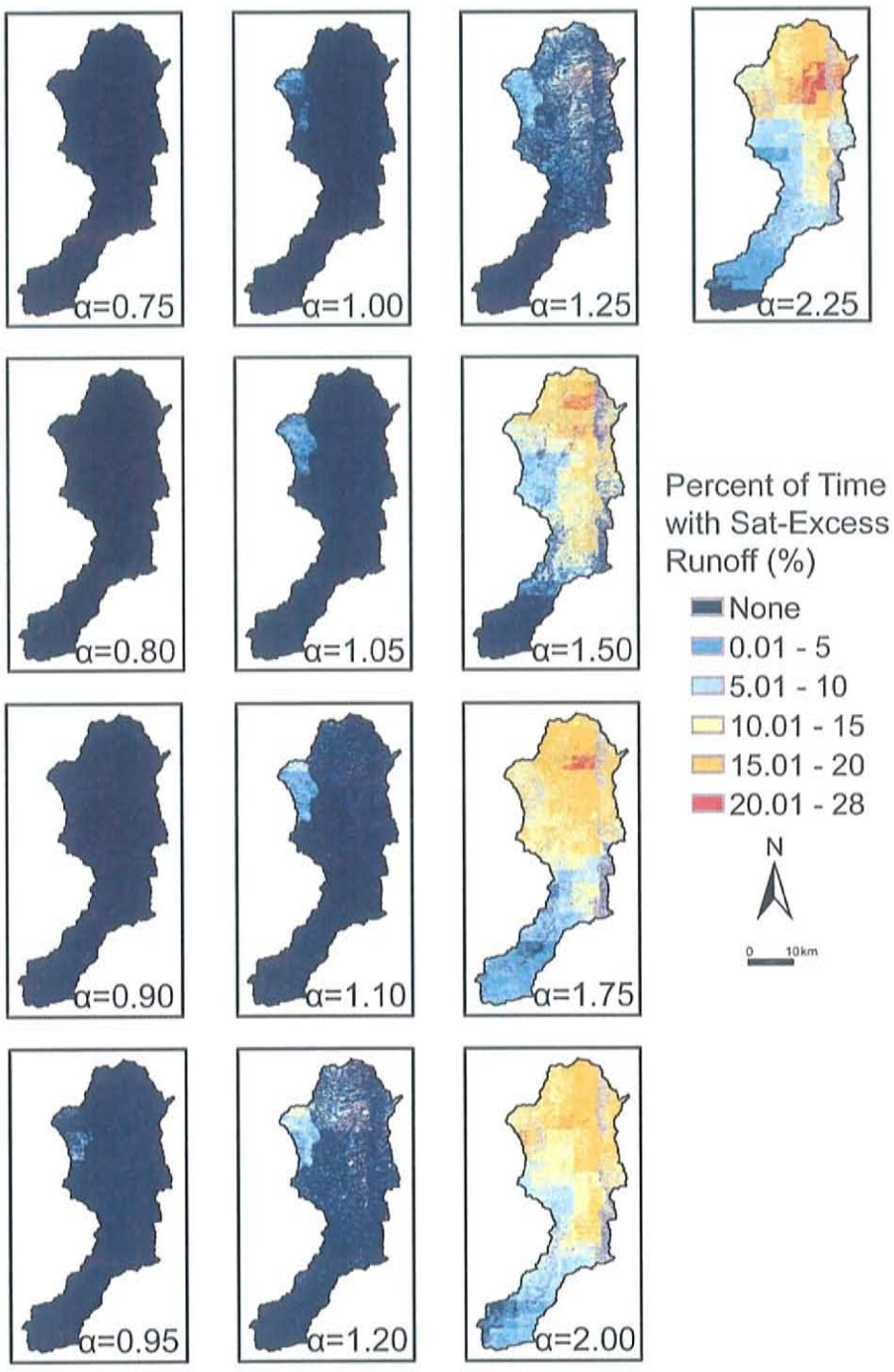


**Figure 2.15.** Spatial distributions of the percent of time with saturation-excess runoff occurrence (%) during September 8-16, 2003, for the adjusted initial soil moisture conditions.

distribution of saturation-excess runoff correlates well with the total rainfall accumulation (Figure 2.10). It is also interesting to note that spatial variability is apparent in the saturation excess runoff due to the land cover or vegetation pattern (see Figure 2.5b). This effect is due to the important role of vegetation in intercepting rainfall and diminishing the intensity observed on the saturated land surface.

Given the observed differences in the hydrologic response for the two sets of ensemble simulations, it is important to summarize how the fixed and adjusted initializations impact the basin response to the imposed rainfall variations. Figure 2.16a compares the runoff ratio ($r = Q/P$) variations with the rainfall volume for the two scenarios. The fixed initialization cases exhibit a linear increase in runoff ratio over the range of total rainfall volume. Note that this increasing trend is less abrupt as compared to the increasing trend for the adjusted initialization cases, despite that both scenarios were forced with the same meteorological fields. For the fixed initialization, once the maximum infiltration capacity is exceeded by the rainfall intensity values, a proportional increase in runoff is produced via the infiltration-excess mechanism. In the adjusted initialization cases, the variation of the groundwater table position used to produce equivalent initial conditions leads to a transition toward saturation-excess runoff. This leads to a faster and non-linear rise in the runoff ratio with imposed increases in rainfall volume. As shown in Figure 2.16b, infiltration-excess runoff is the dominant mechanism for dry initial soil moisture conditions ($s < 0.5$) for rainfall volume less than $3.75 \times 10^7$ m$^3$. Since the initial conditions are matched between the two models, wetter conditions lead to saturation-excess runoff becoming the dominant runoff mechanism ($s > 0.9$) or rainfall volume greater than $5 \times 10^7$ m$^3$. In

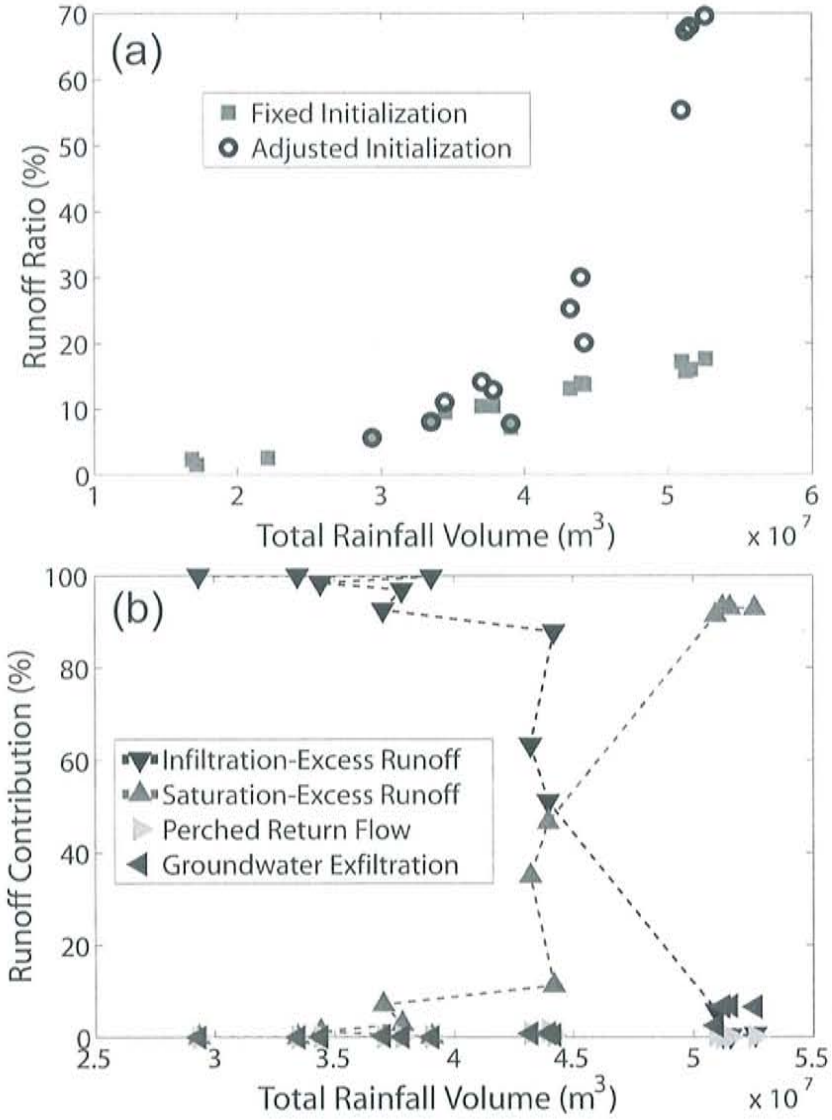


**Figure 2.16.** Effect of rainfall volume on the runoff response. (a) Basin runoff ratio ($r = Q/P$) in Upper Río Puerco outlet for fixed initialization (16 cases) and adjusted initialization (13 cases). (b) Runoff contributions from individual runoff mechanisms as percentage of total runoff (%). Runoff mechanisms include infiltration-excess, saturation-excess, perched return flow and groundwater exfiltration. The runoff contributions are only shown for the adjusted soil moisture initializations between WRF and tRIBS since the fixed initialization yields 100% infiltration-excess runoff for all simulations.

addition, wetter initial conditions slightly increases groundwater exfiltration due to the effect of shallow groundwater near the stream network. For comparison purpose, the fixed initialization conditions exclusively produce infiltration-excess runoff for all rainfall volumes.

The behavior in the two scenarios suggests that the mode of runoff production can significantly change with the antecedent wetness condition (Vivoni et al. 2007c). It also indicates that the basin response can change from a linear (fixed initialization) to a non-linear behavior (adjusted initialization) as a function of initial soil moisture. In particular, the non-linear basin runoff response can be explained by a transition of dominant mechanism from infiltration-excess to saturation-excess runoff. Given the identical meteorological forcings for the two scenarios, we interpret the observed differences in the basin response to be due to the impact of soil moisture initialization on the runoff production mode. This has been observed previously through field and modeling studies. For example, Western et al. (2004) and Merz and Bardossy (1998) found that different spatial patterns of initial soil moisture can produce extremely different results of runoff response even if the spatial statistical distributions of rainfall are similar.

### 2.3.4 Effect of soil moisture initialization on evapotranspiration response

In addition to the notable changes in soil moisture and runoff induced by the regional rainfall, we are interested in how the land surface returns water vapor to the atmosphere. While this is not directly captured in these one-way offline coupled simulations, it is possible to assess variation in evapotranspiration and surface turbulent fluxes. Figure 2.17 presents a comparison of the basin-averaged

evapotranspiration (ET) for the fixed and adjusted initialization conditions. Similar diurnal fluctuations are observed in both scenarios as the simulations of ET are forced by similar meteorological forcings in each ensemble. Note that all the cases, as well as NEXRAD, are close to the ensemble mean ET in the fixed initialization scenario, whereas a wider range is observed among cases for the adjusted initialization, suggesting that the large perturbations in ET are primarily induced by the variation in antecedent soil moisture. The NEXRAD is lower than the ensemble mean of adjusted initializations as it has a lower antecedent wetness for evapotranspiration. In general, the adjusted initializations exhibit greater evapotranspiration and a higher sensitivity to the initial soil moisture ($\alpha$). It is interesting to note that the spread among the adjusted initializations is minimized during the peak runoff production and maximized during the early and final simulation periods, as observed for soil moisture. As expected, this is primarily due to the effect of higher antecedent soil moisture on the soil evaporation and plant transpiration processes in the hydrological model (see Ivanov et al. 2004a). Figure 2.18 presents a comparison of the total evapotranspiration and evapotranspiration ratio ($ET/P$) for the two scenarios. The total ET volume for the fixed initialization cases is nearly constant with increasing rainfall due to relatively small differences in the antecedent soil moisture. In the adjusted initialization cases, however, an increasing trend of ET is observed with higher rainfall as antecedent wetness produces additional water for evapotranspiration from soil and vegetation. Note that the changes in rainfall volume are greater than the changes in ET volume leading to a decreasing trend of ET ratio with rainfall for both scenarios (Figure 2.18b). It is interesting to note this decreasing $ET/P$ trend is less

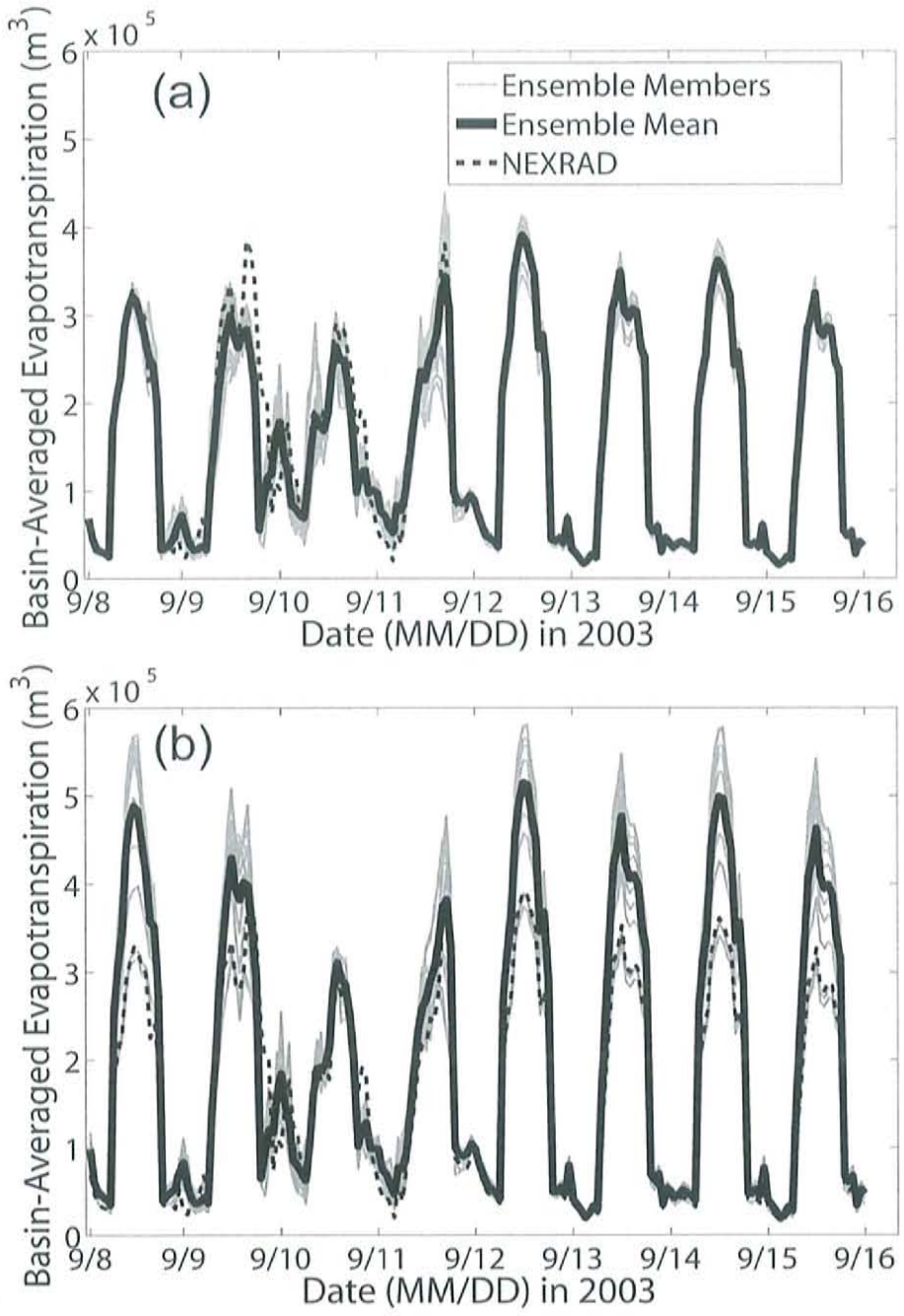


**Figure 2.17.** Comparison of basin-averaged evapotranspiration ($m^3$) for: (a) simulations with different WRF initial soil moisture ($\alpha$ = 0 to 2.25) and fixed initial soil moisture conditions in tRIBS and (b) simulations with adjusted initial soil moisture conditions in tRIBS and WRF ($\alpha$ = 0.75 to 2.25).

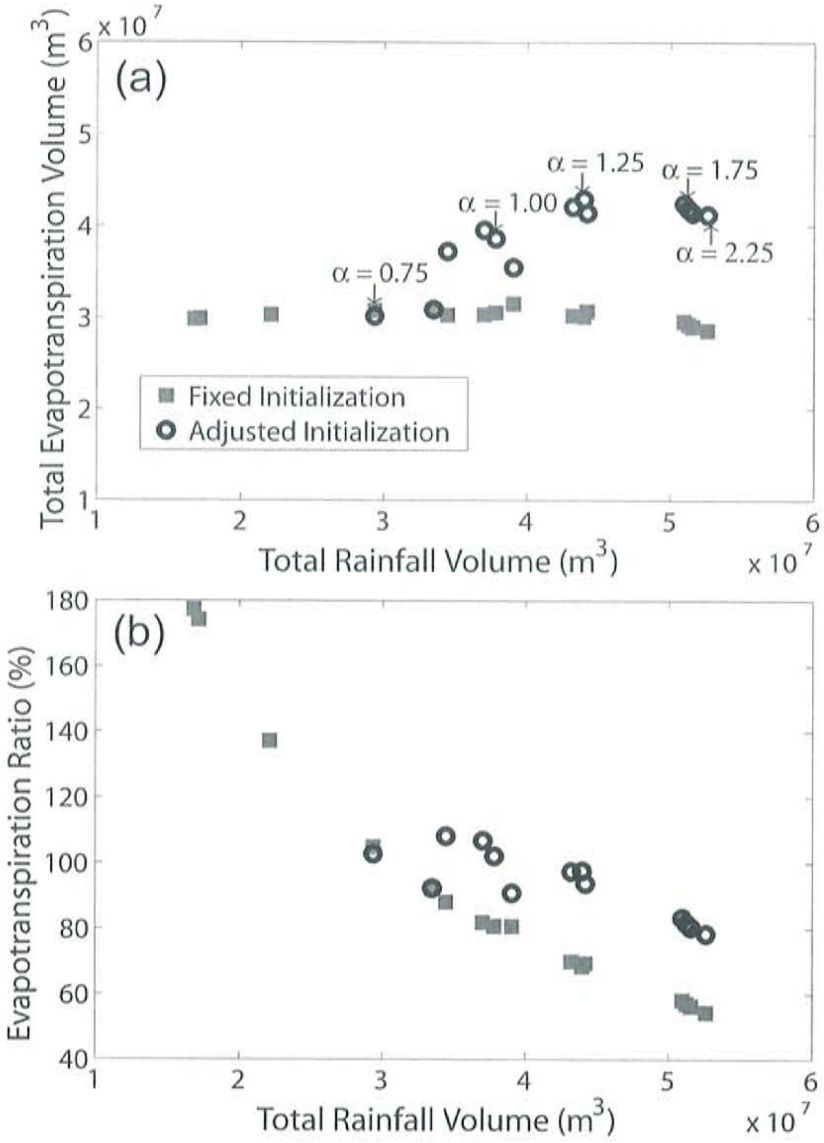


**Figure 2.18.** Effect of rainfall volume on basin evapotranspiration (ET). (a) Total evapotranspiration volume ($m^3$) for fixed (16 cases) and adjusted initializations (13 cases). The labeled cases ($\alpha$ = 0.75, 1.00, 1.25, 1.75 and 2.25) correspond to those presented in Figure 2.17. (b) Evapotranspiration ratio in % (*ET/P*) for the two scenarios.

pronounced for the adjusted initializations as the higher soil moisture promotes greater ET. Ratios of *ET/P* greater than 100% imply that ET consumes available soil water storage (e.g., unsaturated zone moisture or groundwater) beyond the available rainfall during this storm event.

Figure 2.19 presents a comparison of the spatial distributions of evaporative fraction during September 8-16, 2003, for the fixed (left column) and adjusted initializations (right column). Evaporative fraction (EF) is the ratio of surface latent heat exchange ($\lambda E$) rate to total surface turbulent heat exchange ($\lambda E+H$) rate, where $H$ is the sensible heat. Note that the spatial distributions of EF are similar for the fixed initialization cases and match well with the distribution of soil texture, suggesting that the evaporative fraction is influenced by the soil properties under dry initial conditions. In contrast, the adjusted initialization cases exhibit a gradually contrasting distribution of EF with increasing initial soil moisture and correspond to the spatial distribution of vegetation. In particular, the western region of the basin dominated by desert grassland and shrublands has the highest EF, while forested mountains exhibit lower EF. As a result, vegetation type plays an important role in shaping the evapotranspiration process when the initial soil moisture is high. Clearly, the method of initializing the hydrologic model influences the partitioning of surface turbulent fluxes and the return of soil moisture back to the atmosphere. The evapotranspiration process is driven primarily by soil properties under low antecedent soil moisture condition, whereas it is influenced by vegetation properties under increasing antecedent soil moisture conditions.

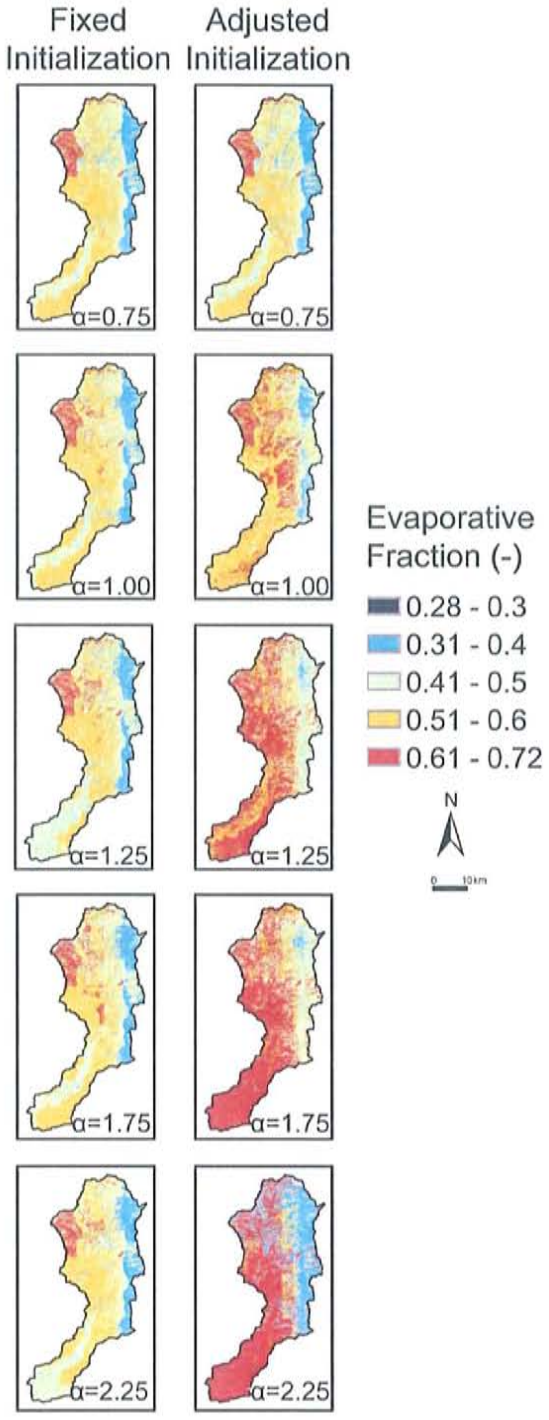


**Figure 2.19.** Effect of initial soil moisture conditions on the evaporative fraction (-) for fixed (left column) and adjusted (right column) initializations. Only a selected number of $\alpha$ cases are shown for clarity.

## 2.4 Conclusions

The primary objective of this paper is to understand how and to what extent initial soil moisture variations impact rainfall generation and its subsequent hydrologic response in the NAM region. In this study, we systematically generated an ensemble of meteorological fields by varying the initial soil moisture conditions in the WRF model. We then focused on analyzing the ensemble rainfall characteristics according to each soil moisture initialization ($\alpha$) in WRF. To study the impact of initializations of the hydrologic model, we tested two scenarios: (1) a fixed soil moisture initialization in tRIBS and (2) adjusted initializations between the tRIBS and WRF models. Subsequently, the basin runoff and evapotranspiration response based upon these two scenarios were compared. Results from the study indicate the following:

(1) The uniform application of a soil moisture multiplier ($\alpha$) in WRF generates a nearly linear increase in the initial soil moisture over all soil depths of the three domains, up to a threshold value of $\alpha = 1.5$. Beyond this range, a non-linear (asymptotic) rise is observed due to the upper limit determined by soil porosity.

(2) The increase in initial soil moisture over a large domain generally increases the total simulated rainfall in our warm-season case study. In particular, the meteorological simulation cases have similar storm timings but varied in the rainfall magnitude, storm location and spatial coverage.

(3) The fixed soil moisture initialization scenario exhibits an increasing runoff ratio with rainfall volume due to the dominance of the infiltration-excess runoff mechanism. The occurrence of infiltration-excess runoff agreed with the spatial

distribution of soil texture. In particular, soil types of low saturated conductivity were found to be more sensitive to rainfall and facilitate frequent infiltration-excess runoff production as compared to permeable soils. This fixed initialization demonstrates the control of both rainfall and soil properties on the spatial distribution of infiltration-excess runoff generation.

(4) The adjusted soil moisture initialization scenario exhibited a runoff ratio that increased more dramatically with rainfall volume due to a transition in runoff mechanisms. In particular, basin runoff production was primarily driven by saturation-excess runoff in the wetter conditions. As a result, both rainfall and initial soil moisture play a dominant role in shaping the basin runoff response with soil properties playing a major role for dry antecedent wetness conditions.

(5) Higher antecedent soil moisture induced by the rainfall scenarios generally increases evapotranspiration response. For low antecedent soil moisture, soil properties play a significant role in shaping the spatial distribution of evapotranspiration process. In contrast, vegetation properties become more influential for the evapotranspiration process for saturated initial soil moisture conditions.

Through the use of the two different scenarios, we demonstrate that the basin runoff response and evapotranspiration differs significantly between dry and wet antecedent soil moisture conditions due to the interplay between different processes occurring in the land surface. Our result is particularly encouraging as it points to the importance of coupled soil moisture-rainfall processes in streamflow and surface flux predictability. Despite this importance, there have been few attempts (Seuffert et al. 2002, Maxwell et al. 2007) in coupling soil moisture, rainfall and hydrologic response

in hydrometeorological modeling system. Moreover, our study illustrates the benefits of using a distributed hydrological model that produces spatiotemporal hydrologic predictions of a series of hydrological variables including runoff production mechanisms and surface flux partitioning.

Our study supports the notion that offline, one-way coupled hydrometeorological models provide new platforms for long-lead time hydrologic forecasts as compared to the traditional use of radar rainfall products. Furthermore, we have demonstrated the value of understanding the influence of initial soil moisture on the rainfall, runoff production and evapotranspiration processes with the combined use of distributed meteorological and hydrological models. Moreover, this study suggests that improved operational assimilation schemes for soil moisture in coupled models is promising and can eventually improve rainfall and streamflow predictability (Schar et al. 1999). A fully two-way coupled hydrometeorological modeling system would be next step toward capturing the soil moisture-rainfall feedback as it would naturally match the soil moisture conditions between the two models.

# CHAPTER 3 SUMMARY AND RECOMMENDATIONS

## 3.1 Summary

In order to understand the impact of varying initial soil moisture on rainfall production and its subsequent hydrologic response in the NAM region, we have presented a systematic approach to create an ensemble of meteorological fields by adjusting initial soil moisture conditions in WRF for a four-day storm event that occurred over the Upper Río Puerco basin in September 2003. The uniform application of soil moisture multipliers to the initial soil moisture condition in WRF led to a nearly linear increase in initial soil moisture over all soil depths of the three domains. We compared the ensemble WRF rainfall simulations over the Upper Río Puerco basin. This comparison indicates that the simulated rainfall and runoff volumes generally increase with initial soil moisture (up to a threshold of initial soil moisture) in our warm-season case study.

We also presented the effect of basin-scale rainfall on hydrologic response based upon two different scenarios: (1) fixed surface soil moisture initializations in tRIBS; and (2) adjusted the surface soil moisture initializations between tRIBS and WRF. The results from both scenarios illustrated that runoff ratio increases with increasing rainfall volume but the increasing trend is more pronounced in the case of adjusted initializations. This difference suggests the runoff response is primarily driven by rainfall intensity in the fixed initialization, while it is the result of both rainfall intensity and antecedent soil moisture conditions in the adjusted initialization.

Infiltration-excess runoff is dominant and responsible for the increase trend of runoff ratio in the fixed initialization case, while a transition from infiltration-excess runoff to saturation-excess runoff is responsible for the transitional runoff behavior in the adjusted initialization case. Furthermore, perturbations in soil moisture initializations cause significant spatial variations in rainfall, runoff production and evapotranspiration. Result from the study indicate the following:

(1) Soil moisture multipliers are uniformly applied in WRF creating a nearly linear increase in initial soil moisture over all soil depths of the three domains, up to a threshold value of $\alpha = 1.5$. Beyond this range, a non-linear (asymptotic) rise is observed due to the upper limit determined by soil porosity.

(2) In our warm-season case study, the total simulated rainfall generally increases with increasing initial soil moisture over a large domain. Moreover, the meteorological simulation cases have similar storm timings but varied in the rainfall magnitude, storm location and spatial coverage.

(3) The scenario based on fixed soil moisture initialization has an increasing runoff ratio with rainfall volume because it is governed by the infiltration-excess runoff mechanism. The occurrence of infiltration-excess runoff agreed with the spatial distribution of soil texture. In particular, soil types of low saturated conductivity were found to be more sensitive to rainfall and facilitate frequent infiltration runoff as compared to soil types with high saturated conductivity. This scenario demonstrates the control of both rainfall and soil properties (i.e., hydraulic conductivity) on the spatial distribution of infiltration-excess runoff generation.

(4) In contrast, the scenario based on adjusted soil moisture initializations demonstrate that the runoff ratio increases more dramatically with rainfall volume and is driven by the transition in runoff mechanisms. In particular, runoff production is primarily driven by saturation-excess runoff in wetter conditions. The initial soil moisture significantly influences the basin runoff response through the interplay between different runoff mechanisms. As a result, both rainfall and initial soil moisture play a dominant role in shaping the basin runoff response.

(5) Higher antecedent soil moisture induced by the rainfall scenarios generally increases evapotranspiration due to water availability. Perturbations in antecedent soil moisture lead to significant changes in evapotranspiration. For low antecedent soil moisture, soil properties play a significant role in shaping the evapotranspiration process, while vegetation properties become more influential for the evapotranspiration process for saturated initial soil moisture conditions.

In conclusion, soil moisture initialization in both weather prediction and hydrological models can significant affect the predictability of rainfall and subsequent hydrologic response. Accurate soil moisture initializations or data assimilation should enhance hydrometeorological predictions.

The synthetic variations in initial soil moisture conditions in all model domains and soil layers in WRF are for the purpose of sensitivity analysis and unrealistic to the nature. Raising the groundwater table close to or at the land surface is also for the purpose of sensitivity analysis and is unrealistic in the URP basin and other semi-arid environments. The input data for WRF is coarse (e.g., coarse soil maps, landuse maps, 32-km NARR data) leading to a potential problem of capturing

some details in the nature. Both the tRIBS and WRF models are limited by the physical parameterizations (e.g., cloud parameterizations in WRF).

### 3.2 Recommendations for Future Work

Our three major recommendations are summarized in the following paragraphs. The first discusses approaches to test the extent of soil moisture variations (i.e. size of domain and soil depths) used to generate an ensemble set of WRF rainfall simulations which is similar to the ensemble in our study. The second consists of testing the effect of vegetation variations on rainfall generation and subsequent hydrologic response. The third emphasizes a need for using a fully-coupled WRF-tRIBS model to properly capture the feedback processes (e.g. soil moisture-rainfall feedback) between the land surface and atmosphere.

In our study, we uniformly applied a set of multipliers to the initial soil moisture condition over all soil depths of all the three WRF domains, for simplicity. Kim and Wang (2007a) examined the role of soil moisture anomalies in deep soil versus those in shallow soil. Their results showed that the persistence of anomalies in the shallow soil is long enough to influence the subsequent rainfall at the seasonal scale, while the deep-soil anomalies further enhance and prolong this persistence. For the purpose of verifying their result, a future study can involve applying only the multipliers to the shallow versus deep layer separately in the WRF model. Another analysis conducted by Kim and Wang (2007a) varied the size or area of the domain over which the soil moisture multipliers were applied. Their result indicates that rainfall response to soil moisture anomalies of the same magnitude on subsequent rainfall can vary significantly with the spatial coverage of such anomalies. For

example, a future experiment can consist of the application of soil moisture multipliers only over the inner domain.

The second recommendation lies on the impact of vegetation dynamics on rainfall production and its subsequent hydrologic response. In this study, we primarily focused on the effect of soil moisture initialization on rainfall, runoff production and evapotranspiration for a constant vegetation canopy. In future studies, it is possible to conduct a similar experiment to our study by varying vegetation dynamics such as greenness fraction (Matsui et al. 2005). This approach would allow testing the extent of changes in vegetation dynamics associated with soil moisture required for significant variations in rainfall and runoff productions. Some researchers have attempted (e.g. Matsui et al. 2005; Kim and Wang 2007b) to examine the impact of vegetation on rainfall production, yet the impact on the runoff generation and evapotranspiration response has not been studied.

Our study indicates the importance of soil moisture initialization for understanding and predicting land-atmosphere processes. As a result, we believe that the future use of a fully coupled WRF-tRIBS system will allow improved simulations of the coupled land-atmosphere system in more sophisticated manner. For example, a fully-coupled WRF-tRIBS hydrometeorological model should properly simulate the coupled soil-vegetation-rainfall processes for improving rainfall and streamflow predictability.

# REFERENCES


Aligo, E. A., W. A. Gallus, and M. Segal, 2007: Summer rainfall forecast spread in an ensemble initialized with different soil moisture analyses. *Weather and Forecasting*, **22,** 299-314.

Beljaars, A. C. M., P. Viterbo, M. J. Miller, and A. K. Betts, 1996: The anomalous rainfall over the United States during July 1993: Sensitivity to land surface parameterization and soil moisture. *Monthly Weather Review*, **124,** 362-383.

Benjamin, S. G. and T. N. Carlson, 1986: Some effects of surface heating and topography on the regional severe storm environment. 1. Three-dimensional simulations. *Monthly Weather Review*, **114,** 307-329.

Beven, K.J. 2002. Runoff Generation in Semi-arid Areas. In: L.J. Bull and M.J. Kirkby (Eds.), Dryland Rivers: *Hydrology and Geomorphology of Semi-arid Channels*, John Wiley and Sons: New York, 57- 105.

Bosilovich, M. G. and W. Y. Sun, 1999: Numerical simulation of the 1993 midwestern flood: Local and remote sources of water. *Journal of Geophysical Research-Atmospheres*, **104,** 19415-19423.

Castillo, V. M., A. Gomez-Plaza, and M. Martinez-Mena, 2003: The role of antecedent soil water content in the runoff response of semiarid catchments: a simulation approach. *Journal of Hydrology*, **284**, 114-130.

Chancibault, K., S. Anquetin, V. Ducrocq, and G. M. Saulnier, 2006: Hydrological evaluation of high-resolution precipitation forecasts of the Gard flash-flood event

(8-9 September 2002). *Quarterly Journal of the Royal Meteorological Society*, **132,** 1091-1117.

Chen, F. and J. Dudhia, 2001: Coupling an advanced land surface-hydrology model with the Penn State-NCAR MM5 modeling system. Part I: Model implementation and sensitivity. *Monthly Weather Review*, **129,** 569-585.

Decharme, B. and H. Douville, 2006: Uncertainties in the GSWP-2 precipitation forcing and their impacts on regional and global hydrological simulations. *Climate Dynamics*, **27,** 695-713.

Dudhia, J., 1989: Numerical study of convection observed during the winter monsoon experiment using a mesoscale two-dimensional model. *Journal of the Atmospheric Sciences*, **46,** 3077-3107.

Eltahir, E. A. B., 1998: A soil moisture rainfall feedback mechanism 1. Theory and observations. *Water Resources Research*, **34,** 765-776.

Gao, X., J. Li, and S. Sorooshian, 2007: Modeling intraseasonal features of 2004 North American monsoon precipitation. *Journal of Climate*, **20,** 1882-1896.

Gochis, D. J., W. J. A. Shuttleworth, and Z. L. Yang, 2002: Sensitivity of the modeled North American monsoon regional climate to convective parameterization. *Monthly Weather Review*, **130,** 1282-1298.

Gochis, D. J., W. J. Shuttleworth, and Z. L. Yang, 2003: Hydrometeorological response of the modeled North American monsoon to convective parameterization. *Journal of Hydrometeorology*, **4,** 235-250.

Griffin, E. R., J. W. Kean, K. R. Vincent, J. D. Smith, and J. M. Friedman, 2005: Modeling effects of bank friction and woody bank vegetation on channel flow and

boundary shear stress in the Río Puerco, New Mexico. *Journal of Geophysical Research-Earth Surface*, **110**. F04023, doi:10.1029/2005JF000322.

Hay, L. E., M. P. Clark, M. Pagowski, G. H. Leavesley, and W. J. Gutowski, 2006: One-way coupling of an atmospheric and a hydrologic model in Colorado. *Journal of Hydrometeorology*, **7**, 569-589.

Higgins, R. W., A. Douglas, A. Hahmann, E. H. Berbery, D. Gutzler, J. Shuttleworth, D. Stensrud, J. Amador, R. Carbone, M. Cortez, M. Douglas, R. Lobato, J. Meitin, C. Ropelewski, J. Schemm, S. Schubert, and C. D. Zhang, 2003: Progress in Pan American CLIVAR Research: The North American Monsoon System. *Atmosfera*, **16,** 29-65.

Hong, S. Y. and H. L. Pan, 2000: Impact of soil moisture anomalies on seasonal, summertime circulation over North America in a Regional Climate Model. *Journal of Geophysical Research-Atmospheres*, **105,** 29625-29634.

Ivanov, V. Y., E. R. Vivoni, R. L. Bras and D. Entekhabi, 2004a: Catchment hydrologic response with a fully-distributed triangulated irregular network model. *Water Resources Research*, **40**, W11102, doi:10.1029/2004WR003218.

Ivanov, V. Y., E. R. Vivoni, R. L. Bras, and D. Entekhabi, 2004b: Preserving high-resolution surface and rainfall data in operational-scale basin hydrology: a fully-distributed physically-based approach. *Journal of Hydrology*, **298,** 80-111.

Janjic, Z. I., 2002: *Nonsingular implementation of the Mellor-Yamada level 2.5 scheme in the NCEP Meso model*. NCEP Office Note 437, 61 pp. [Available online at http://www.emc.ncep.noaa.gov/officenotes/FullTOC.html.]

Kain, J. S. and J. M. Fritsch, 1990: A one-dimensional entraining detraining plume

model and its application in convective parameterization. *Journal of the Atmospheric Sciences*, **47,** 2784-2802.

Kim, Y. and G. L. Wang, 2007a: Impact of initial soil moisture anomalies on subsequent precipitation over North America in the coupled land-atmosphere model CAM3-CLM3. *Journal of Hydrometeorology*, **8,** 513-533.

Kim, Y. and G. L. Wang, 2007b: Impact of vegetation feedback on the response of precipitation to antecedent soil moisture anomalies over North America. *Journal of Hydrometeorology*, **8,** 534-550.

Koster, R. D., P. A. Dirmeyer, Z. C. Guo, G. Bonan, E. Chan, P. Cox, C. T. Gordon, S. Kanae, E. Kowalczyk, D. Lawrence, P. Liu, C. H. Lu, S. Malyshev, B. McAvaney, K. Mitchell, D. Mocko, T. Oki, K. Oleson, A. Pitman, Y. C. Sud, C. M. Taylor, D. Verseghy, R. Vasic, Y. K. Xue, T. Yamada, and G. Team, 2004: Regions of strong coupling between soil moisture and precipitation. *Science*, **305,** 1138-1140.

Kurc, S. A. and E. E. Small, 2007: Soil moisture variations and ecosystem-scale fluxes of water and carbon in semiarid grassland and shrubland. *Water Resources Research*, **43**, W06416, doi:10.1029/2006WR005011.

Lanicci, J. M., T. N. Carlson, and T. T. Warner, 1987: Sensitivity of the Great-Plains severe-storm environment to soil-moisture distribution. *Monthly Weather Review*, **115,** 2660-2673.

Lin, C. A., L. Wen, G. H. Lu, Z. Y. Wu, J. Y. Zhang, Y. Yang, Y. F. Zhu, and L. Y. Tong, 2006: Atmospheric-hydrological modeling of severe precipitation and floods in the Huaihe River Basin, China. *Journal of Hydrology*, **330,** 249-259.

Mahfouf, J. F., 1991: Analysis of soil-moisture from near-surface parameters – A feasibility study. *Journal of Applied Meteorology*, **30,** 1534-1547.

Marani, M., E. Eltahir, and A. Rinaldo, 2001: Geomorphic controls on regional base flow. *Water Resources Research*, **37,** 2619-2630.

Matsui, T., V. Lakshmi, and E. E. Small, 2005: The effects of satellite-derived vegetation cover variability on simulated land-atmosphere interactions in the NAMS. *Journal of Climate*, **18,** 21-40.

Maxwell, R. M., F. K. Chow, and S. J. Kollet, 2007: The groundwater-land-surface-atmosphere connection: Soil moisture effects on the atmospheric boundary layer in fully-coupled simulations. *Advances in Water Resources*, **30**, 2447-2466.

Merz, B. and A. Bardossy, 1998: Effects of spatial variability on the rainfall runoff process in a small loess catchment. *Journal of Hydrology*, **213**, 304-317.

Mesinger, F., G. DiMego, E. Kalnay, K. Mitchell, P. C. Shafran, W. Ebisuzaki, D. Jovic, J. Woollen, E. Rogers, E. H. Berbery, M. B. Ek, Y. Fan, R. Grumbine, W. Higgins, H. Li, Y. Lin, G. Manikin, D. Parrish, and W. Shi, 2006: North American regional reanalysis. *Bulletin of the American Meteorological Society*, **87,** 343.

Mintz, Y., 1984: The sensitivity of numerically simulated climates to land-surface boundary conditions. In Hoyughton, J. T. (Ed.). *The Global Climate,* pp. 79-105. Cambridge University Press, Cambridge, UK.

Miyakoda, K., G. D. Hembree, and R. F. Strickler, 1979: Cumulative results of extended forecast experiments. 2. Model performance for summer cases. *Monthly Weather Review*, **107,** 395-420.

Mlawer, E. J., S. J. Taubman, P. D. Brown, M. J. Iacono, and S. A. Clough, 1997: Radiative transfer for inhomogeneous atmospheres: RRTM, a validated correlated-k model for the longwave. *Journal of Geophysical Research-Atmospheres*, **102,** 16663-16682.

Mo, K. C., J. E. Schemm, H. Kim, and W. R. Higgins, 2006: Influence of initial conditions on summer precipitation simulations over the United States and Mexico. *Journal of Climate*, **19,** 3640-3658.

Oglesby R. J., S. Marshall, D. J. Erickson III, J. O. Roads, and F. R. Robertson, 2002: Thresholds in atmosphere–soil moisture interactions: Results from climate model studies. *Journal of Geophysical Research-Atmospheres*, **107**, 4224, doi:10.1029/2001JD001045.

Pal, J. S. and E. A. B. Eltahir, 2001: Pathways relating soil moisture conditions to future summer rainfall within a model of the land-atmosphere system. *Journal of Climate*, **14,** 1227-1242.

Ratnam, J. V. and K. K. Kumar, 2005: Sensitivity of the simulated monsoons of 1987 and 1988 to convective parameterization schemes in MM5. *Journal of Climate*, **18,** 2724-2743.

Reed, S., V. Koren, M. Smith, Z. Zhang, F. Moreda, D. J. Seo, and D. Participants, 2004: Overall distributed model intercomparison project results. *Journal of Hydrology*, **298,** 27-60.

Rowntree, P. R. and J. A. Bolton, 1983: Simulation of the atmospheric response to soil-moisture anomalies over Europe. *Quarterly Journal of the Royal Meteorological Society*, **109,** 501-526.

Skamarock, W. C., J. B. Klemp, J. Dudhia, D. O. Gill, D. M. Barker, W. Wang, and J. G. Powers, 2005: *A description of the advanced research WRF version 2*. NCAR Tech. Note NCAR/TN-468STR, 88 pp. [Available online at http://www.wrf-model.org/wrfadmin/docs/arw_v2.pdf.]

Schar, C., D. Luthi, U. Beyerle, and E. Heise, 1999: The soil-precipitation feedback: A process study with a regional climate model. *Journal of Climate*, **12,** 722-741.

Schubert, S. D., M. J. Suarez, P. J. Pegion, R. D. Koster, and J. T. Bacmeister, 2004: On the cause of the 1930s Dust Bowl. *Science*, **303,** 1855-1859.

Seuffert, G., P. Gross, C. Simmer, and E. F. Wood, 2002: The influence of hydrologic modeling on the predicted local weather: Two-way coupling of a mesoscale weather prediction model and a land surface hydrologic model. *Journal of Hydrometeorology*, **3,** 505-523.

Small, E. E., 2001: The influence of soil moisture anomalies on variability of the North American monsoon system, *Geophysical Research Letters*, **28**, 139-142.

Sutton, C., T. M. Hamill, and T. T. Warner, 2006: Will perturbing soil moisture improve warm-season ensemble forecasts? A proof of concept. *Monthly Weather Review*, **134,** 3174-3189.

Thompson, G., R. M. Rasmussen, and K. Manning, 2004: Explicit forecasts of winter precipitation using an improved bulk microphysics scheme. Part I: Description and sensitivity analysis. *Monthly Weather Review*, **132,** 519-542.

Vera, C., W. Higgins, J. Amador, T. Ambrizzi, R. Garreaud, D. Gochis, D. Gutzler, D. Lettenmaier, J. Marengo, C. R. Mechoso, J. Nogues-Paegle, P. L. S. Dias, and C. Zhang, 2006: Toward a unified view of the American Monsoon Systems.

*Journal of Climate*, **19,** 4977-5000.

Vivoni, E. R., V. Y. Ivanov, R. L. Bras, and D. Entekhabi, 2004: Generation of triangulated irregular networks based on hydrological similarity. *Journal of Hydrologic Engineering*, **9**, 288-302.

Vivoni, E. R., V. Y. Ivanov, R. L. Bras, and D. Entekhabi, 2005: On the effects of triangulated terrain resolution on distributed hydrologic model response. *Hydrological Processes*, **19**, 2101-2122.

Vivoni, E. R., R. S. Bowman, R. L. Wyckoff, R. T. Jakubowski, and K. E. Richards, 2006: Analysis of a monsoon flood event in an ephemeral tributary and its downstream hydrologic effects. *Water Resources Research*, **42**. W03404, doi:10.1029/2005WR004036.

Vivoni, E. R., D. Entekhabi, R. L. Bras, V. Y. Ivanov, M. P. Van Horne, C. Grassotti, and R. N. Hoffman, 2006: Extending the predictability of hydrometeorological flood events using radar rainfall nowcasting. *Journal of Hydrometeorology*, 7, 660-677.

Vivoni, E. R., H. A. Gutiérrez-Jurado, C. A. Aragón, L. A. Méndez-Barroso, A. J. Rinehart, R. L. Wyckoff, J. C. Rodríguez, C. J. Watts, J. D. Bolten, V. Lakshmi, and T. J. Jackson, 2007a: Variation of hydrometeorological conditions along a topographic transect in northwestern Mexico during the North American monsoon. *Journal of Climate,* **20**, 1792-1809.

Vivoni, E. R., D. Entekhabi, and R. N. Hoffman, 2007b: Error propagation of radar rainfall nowcasting fields through a fully distributed flood forecasting model. *Journal of Applied Meteorology and Climatology*, **46,** 932-940.

Vivoni, E.R., D. Entekhabi, R. L Bras, and V. Y. Ivanov, 2007c: Controls on runoff generation and scale-dependence in a distributed hydrologic model. *Hydrology and Earth System Sciences*, **11**, 1683-1701.

Wang, G. L., Y. Kim, and D. G. Wang, 2007: Quantifying the strength of soil moisture-precipitation coupling and its sensitivity to changes in surface water budget. *Journal of Hydrometeorology*, **8,** 551-570.

Western, A. W., S. L. Zhou, R. B. Grayson, T. A. McMahon, G. Bloschl, and D. J. Wilson, 2004: Spatial correlation of soil moisture in small catchments and its relationship to dominant spatial hydrological processes. *Journal of Hydrology*, **286**, 113-134.

Westrick, K. J. and C. F. Mass, 2001: An evaluation of a high-resolution hydrometeorological modeling system for prediction of a cool-season flood event in a coastal mountainous watershed. *Journal of Hydrometeorology*, **2**, 161-180.

Williams, W. A., M. E. Jensen, J. C. Winne, and R. L. Redmond, 2000: An automated technique for delineating and characterizing valley-bottom settings. *Environmental Monitoring and Assessment*, **64**, 105-114.

Wyckoff, R. L., 2007: *Sensitivity to arroyo development scenarios: Insights from a distributed hydrologic model.* Master thesis, New Mexico Institute of Mining and Technology, 193 pp.

Xie, H. J., X. B. Zhou, E. R. Vivoni, J. M. H. Hendrickx, and E. E. Small, 2005: GIS-based NEXRAD Stage III precipitation database: automated approaches for data processing and visualization. *Computers & Geosciences*, **31,** 65-76.

Xu, J. J. and E. E. Small, 2002: Simulating summertime rainfall variability in the

North American monsoon region: The influence of convection and radiation parameterizations. *Journal of Geophysical Research-Atmospheres*, **107 (D23)**, 4727, doi:10.1029/2001JD002047.

Xu, J. J., W. J. Shuttleworth, X. Gao, S. Sorooshian, and E. E. Small, 2004: Soil moisture-precipitation feedback on the North American monsoon system in the MM5-OSU model. *Quarterly Journal of the Royal Meteorological Society*, **130,** 2873-2890.

Yates, D. N., T. T. Warner, and G. H. Leavesley, 2000: Prediction of a flash flood in complex terrain. Part II: A comparison of flood discharge simulations using rainfall input from radar, a dynamic model, and an automated algorithmic system. *Journal of Applied Meteorology*, **39,** 815-825.

Zheng, X. Y. and E. A. B. Eltahir, 1998a: A soil moisture rainfall feedback mechanism 2. Numerical experiments. *Water Resources Research*, **34,** 777-785.

Zheng, X. Y. and E. A. B. Eltahir, 1998b: The role of vegetation in the dynamics of West African monsoons. *Journal of Climate*, **11,** 2078-2096.

Zhu, C., T. Cavazos and D. P. Lettenmaier, 2007: Role of antecedent land surface conditions in warm season precipitation over northwestern Mexico. *Journal of Climate*, **20**, 1774-1791.

# APPENDICES

## A.1 Outline of Data Structure

The program flow of meteorological and hydrologic modeling is in this sequence: (1) WRF Preprocessing System called "WPS", (2) WRF, (3) Post-processing for WRF meteorological outputs and (4) tRIBS. The following sections outline the input and output datasets related to each program in the order of the modeling sequence. Pathnames to model input data found in the initialization or run files may require slight modifications prior to performing WRF or tRIBS simulations.

A.2 WRF Preprocessing System (WPS)

A.2.1 In Files → Simulation Input Files

A.2.2 Input_Data → Required Modeling Datasets

A.2.3 Model Output → Simulation Folders

A.3 WRF Model Simulations

A.3.1 In Files → Simulation Input Files

A.3.2 Input_Data → Required Modeling Datasets

A.3.3 Model Output → Simulation Folders

A.4 tRIBS for the Fixed Initializations

A.4.1 In Files → Simulation Input Files

A.4.2 Input_Data → Required Modeling Datasets

A.4.3 Model Output → Simulation Folders

A.5 tRIBS for the Adjusted Initializations

A.5.1 In Files → Simulation Input Files

A.5.2 Input_Data → Required Modeling Datasets

A.5.3 Model Output → Simulation Folders

A.6 IDL Script for Postprocessing WRF outputs for tRIBS

## A.2 WRF Preprocessing System (WPS)

A.2.1 In File

- /model-out/ is attached to riogrande.nmt.edu
- Folder's Path: /model-out/tai_data/wps/in_file/
- namelist.wps is read and required by WPS.

A.2.2 Input_Data

- Folder's Path: /model-out/tai_data/wps/input_data/
- The following table describes WPS datasets used for preparing input to WRF.

**Table A.1** Input datasets in WPS.

| File Name | Data Description |
|---|---|
| geog.tar.gz | Terrestrial Input Data |
| narr.tar.gz | North America Regional Reanalysis for Initial and Boundary Conditions |

A.2.3 Model Output

- Folder's Path: /model-out/tai_data/wps/model_output/
- The following WPS output dataset provides input to WRF.

**Table A.2** Model output datasets in the WPS.

| File Name | Data Description |
|---|---|
| met_em.tar.gz | Meteorological input data for WRF |

### A.3 WRF Model Simulations

We applied a particular soil moisture multiplier, $\alpha$ on line 1090 of the code inside WRF/share/module_soil_pre.F. For example, we multiplied the soil moisture by a multiplier, $\alpha$ of 2.25 by putting "*2.25" on the code. This modification of $\alpha$ is highlighted in the following portion of module_soil_pre.F:

```
! Interpolate between the layers we have (zhave) and those that we want (zs).
z_wantm : DO lwant = 1 , num_soil_layers
  z_havem : DO lhave = 1 , num_sm_levels_input +2 -1
    IF ( ( zs(lwant) .GE. zhave(lhave  ) ) .AND. &
       ( zs(lwant) .LE. zhave(lhave+1) ) ) THEN
      DO j = jts , MIN(jde-1,jte)
        DO i = its , MIN(ide-1,ite)
          smois(i,lwant,j)= ( sm_input(i,lhave  ,j) * ( zhave(lhave+1) - zs   (lwant) ) + &
                        sm_input(i,lhave+1,j) * ( zs   (lwant  ) - zhave(lhave) ) ) / &
                                        ( zhave(lhave+1) - zhave(lhave) )
          smois(i,lwant,j) = smois(i,lwant,j)*2.25
          IF (smois(i,lwant,j) .GT. 1) THEN
            smois(i,lwant,j) = 1
          END IF
        END DO
      END DO
      EXIT z_havem
    END IF
  END DO z_havem
```

After making this modification on the code, we recompiled WRF to perform the simulation correspondingly to a particular $\alpha$.

### A.3.1 In File

- Folder's Path: /model-out/tai_data/wrf/in_file/
- namelist.input is the same for all WRF ensemble simulations.

### A.3.2 Input_Data

- Folder's Path: /model-out/tai_data/wrf/input_data/
- The following input data from WPS is required for WRF simulation.

**Table A.3** Input datasets in WRF.

| File Name | Data Description |
|---|---|
| met_em.tar.gz | Meteorological input data for WRF |

A.3.3 Model Output

- Folder's Path: /model-out/tai_data/wrf/model_output/
- The following WRF output datasets are based on various soil moisture multipliers, $\alpha$.

**Table A.4** Model output datasets in WRF.

| File Name | Data Description |
|---|---|
| wrfout_a1.tar.gz | WRF Meteorological output data for $\alpha = 0.00$ |
| wrfout_a2.tar.gz | WRF Meteorological output data for $\alpha = 0.20$ |
| wrfout_a3.tar.gz | WRF Meteorological output data for $\alpha = 0.50$ |
| wrfout_a4.tar.gz | WRF Meteorological output data for $\alpha = 0.75$ |
| wrfout_a5.tar.gz | WRF Meteorological output data for $\alpha = 0.80$ |
| wrfout_a6.tar.gz | WRF Meteorological output data for $\alpha = 0.90$ |
| wrfout_a7.tar.gz | WRF Meteorological output data for $\alpha = 0.95$ |
| wrfout_a8.tar.gz | WRF Meteorological output data for $\alpha = 1.00$ |
| wrfout_a9.tar.gz | WRF Meteorological output data for $\alpha = 1.05$ |
| wrfout_a10.tar.gz | WRF Meteorological output data for $\alpha = 1.10$ |
| wrfout_a11.tar.gz | WRF Meteorological output data for $\alpha = 1.20$ |
| wrfout_a12.tar.gz | WRF Meteorological output data for $\alpha = 1.25$ |
| wrfout_a13.tar.gz | WRF Meteorological output data for $\alpha = 1.50$ |
| wrfout_a14.tar.gz | WRF Meteorological output data for $\alpha = 1.75$ |
| wrfout_a15.tar.gz | WRF Meteorological output data for $\alpha = 2.00$ |
| wrfout_a16.tar.gz | WRF Meteorological output data for $\alpha = 2.25$ |

## A.4 tRIBS for the Fixed Initializations

### A.4.1 In File

- Folder's Path: /model-out/tai_data/tribs/a_16/in_file/
- The following In Files are required for tRIBS ensemble simulations.

**Table A.5** Model run files for tRIBS simulations with fixed initializations.

| In File Name | α |
|---|---|
| spa_0.0 | 0.00 |
| spa_0.2 | 0.20 |
| spa_0.5 | 0.50 |
| spa_0.75 | 0.75 |
| spa_0.8 | 0.80 |
| spa_0.9 | 0.90 |
| spa_0.95 | 0.95 |
| spa_1.0 | 1.00 |
| spa_1.05 | 1.05 |
| spa_1.1 | 1.10 |
| spa_1.2 | 1.20 |
| spa_1.25 | 1.25 |
| spa_1.5 | 1.50 |
| spa_1.75 | 1.75 |
| spa_2.0 | 2.00 |
| spa_2.25 | 2.25 |

### A.4.2 Input_Data

- Folder's Path: /model-out/tai_data/tribs/a_16/input_data/Input/
- The following table describes the input datasets required for tRIBS model initial conditions and model simulations.

**Table A.6** Input datasets for tRIBS simulations with fixed initializations.

| Sub-Directory | FileName | Data Description |
|---|---|---|
| Bedrock | sep25_06_mbrd.brd | Depth to Bedrock |
| GW | 54000_5mlow.iwt | Initial Water Table |
| LandUse | urptw_lu_recl.lan | Land Use Map |
| | urptw_lu_rel.ldt | Land Use Parameters |
| Soils | oct06_soils_reclass.soi | Soil Texture Map |
| | apr17a_soils_reclass.sdt | Soil Parameters |
| Nodes | oNodes.dat | Interior Hydrograph Output Nodes |
| | pNodes.nol | Dynamic Output Nodes |
| PointFiles | urp_z_10_new. points | tRIBS Points File |

- Folder's Path: /model-out/tai_data/tribs/a_16/input_data/Weather/
- The following table describes the WRF input datasets required for tRIBS simulations.

**Table A.7** Meteorological inputs for tRIBS simulations with fixed initializations.

| Sub-Directory | Data Description | α |
|---|---|---|
| out_0.0 | WRF Meteorological Fields including Pressure, Rainfall, Relative Humidity, Sky Cover, Temperature and Wind Speed. | 0.00 |
| out _0.2 | | 0.20 |
| out _0.5 | | 0.50 |
| out _0.75 | | 0.75 |
| out _0.8 | | 0.80 |
| out _0.9 | | 0.90 |
| out _0.95 | | 0.95 |
| out _1.0 | | 1.00 |
| out _1.05 | | 1.05 |
| out _1.1 | | 1.10 |
| out _1.2 | | 1.20 |
| out _1.25 | | 1.25 |
| out _1.5 | | 1.50 |
| out _1.75 | | 1.75 |
| out _2.0 | | 2.00 |
| out _2.25 | | 2.25 |

A.4.3 Model Output

- Folder's Path: /model-out/tai_data/tribs/a_16/model_output/spa/
- The following tRIBS output datasets are based on various soil moisture multipliers, α.

**Table A.8** Model output datasets for tRIBS simulations with fixed initializations.

| Output Folder | $\alpha$ |
|---|---|
| 0.0 | 0.00 |
| 0.2 | 0.20 |
| 0.5 | 0.50 |
| 0.75 | 0.75 |
| 0.8 | 0.80 |
| 0.9 | 0.90 |
| 0.95 | 0.95 |
| 1.0 | 1.00 |
| 1.05 | 1.05 |
| 1.1 | 1.10 |
| 1.2 | 1.20 |
| 1.25 | 1.25 |
| 1.5 | 1.50 |
| 1.75 | 1.75 |
| 2.0 | 2.00 |
| 2.25 | 2.25 |

## A.5 tRIBS for the Adjusted Initializations

### A.5.1 In File

- Folder's Path: /model-out/tai_data/tribs/b_13/in_file/
- The following In Files are required for tRIBS ensemble simulations.

**Table A.9** Model run files for tRIBS simulations with adjusted initializations.

| In File Name | $\alpha$ |
|---|---|
| spa_0.75 | 0.75 |
| spa_0.8 | 0.80 |
| spa_0.9 | 0.90 |
| spa_0.95 | 0.95 |
| spa_1.0 | 1.00 |
| spa_1.05 | 1.05 |
| spa_1.1 | 1.10 |
| spa_1.2 | 1.20 |
| spa_1.25 | 1.25 |
| spa_1.5 | 1.50 |
| spa_1.75 | 1.75 |
| spa_2.0 | 2.00 |
| spa_2.25 | 2.25 |

A.5.2 Input_Data

- Folder's Path: /model-out/tai_data/tribs/b_13/input_data/Input/
- The following table describes the input datasets required for tRIBS model initial conditions and model simulations.

**Table A.10** Input datasets for tRIBS simulations with adjusted initializations.

| Sub-Directory | FileName | Data Description |
|---|---|---|
| Bedrock | sep25_06_mbrd.brd | Depth to Bedrock |
| GW | *.iwt for various $\alpha$ | Initial Water Table |
| LandUse | urptw_lu_recl.lan | Land Use Map |
| | urptw_lu_rel.ldt | Land Use Parameters |
| Soils | oct06_soils_reclass.soi | Soil Texture Map |
| | apr17a_soils_reclass.sdt | Soil Parameters |
| Nodes | oNodes.dat | Interior Hydrograph Output Nodes |
| | pNodes.nol | Dynamic Output Nodes |
| PointFiles | urp_z_10_new. points | tRIBS Points File |

- Folder's Path: /model-out/tai_data/tribs/b_13/input_data/Input/GW/
- The following table describes the initial groundwater input datasets required for tRIBS simulations based on various $\alpha$.

**Table A.11** Initial groundwater inputs for tRIBS simulations with adjusted initializations.

| IWT File | $\alpha$ |
|---|---|
| 7k.iwt | 0.75 |
| 54000_5mlow.iwt | 0.80 |
| 2k.iwt | 0.90 |
| m3750.iwt | 0.95 |
| 1k.iwt | 1.00 |
| m4200.iwt | 1.05 |
| p5k.iwt | 1.10 |
| m4750.iwt | 1.20 |
| m4900.iwt | 1.25 |
| m5350.iwt | 1.50 |
| m8k.iwt | 1.75 |
| m8k.iwt | 2.00 |
| m8k.iwt | 2.25 |

- Folder's Path: /model-out/tai_data/tribs/b_13/input_data/Weather/
- The following table describes the WRF input datasets required for tRIBS simulations.

**Table A.12** Meteorological inputs for tRIBS simulations with adjusted initializations.

| Sub-Directory | Data Description | α |
|---|---|---|
| out _0.75 | WRF Meteorological Fields including Pressure, Rainfall, Relative Humidity, Sky Cover, Temperature and Wind Speed. | 0.75 |
| out _0.8 | | 0.80 |
| out _0.9 | | 0.90 |
| out _0.95 | | 0.95 |
| out _1.0 | | 1.00 |
| out _1.05 | | 1.05 |
| out _1.1 | | 1.10 |
| out _1.2 | | 1.20 |
| out _1.25 | | 1.25 |
| out _1.5 | | 1.50 |
| out _1.75 | | 1.75 |
| out _2.0 | | 2.00 |
| out _2.25 | | 2.25 |

A.5.3 Model Output

- Folder's Path: /model-out/tai_data/tribs/b_13/model_output/spa/
- The following tRIBS output datasets are based on various soil moisture multipliers, $\alpha$.

**Table A.13** Model output datasets for tRIBS simulations with adjusted initializations.

| Output Folder | $\alpha$ |
|---|---|
| 0.75 | 0.75 |
| 0.8 | 0.80 |
| 0.9 | 0.90 |
| 0.95 | 0.95 |
| 1.0 | 1.00 |
| 1.05 | 1.05 |
| 1.1 | 1.10 |
| 1.2 | 1.20 |
| 1.25 | 1.25 |
| 1.5 | 1.50 |
| 1.75 | 1.75 |
| 2.0 | 2.00 |
| 2.25 | 2.25 |

## A.6 IDL Script for Postprocessing WRF outputs for tRIBS

- Folder's Path: /model-out/tai_data/idl_code/wrf.pro

```
pro wrf,directoryIn,directoryOut,lumped=lumped

if keyword_set(lumped) then begin
        cd,directoryIn

        outputFiles=(file_search('*'))[0]

        id = NCDF_OPEN( outputFiles , /NOWRITE)

        NCDF_ATTGET, id, /GLOBAL, 'CEN_LAT', cen_lat
        NCDF_ATTGET, id, /GLOBAL, 'CEN_LON', cen_lon
        NCDF_ATTGET, id, /GLOBAL, 'DY', res_lat
        NCDF_ATTGET, id, /GLOBAL, 'DX', res_lon
        NCDF_ATTGET, id, /GLOBAL, 'DT', dt
        NCDF_ATTGET, id, /GLOBAL, 'START_DATE', start_date

        start_date=string(start_date)
        start_date=strsplit(start_date,'[-_:]',/regex,/EXTRACT)
        fileMM=start_date[1]
        fileDD=start_date[2]
        fileYY=start_date[0]
        fileHH=start_date[3]

        utmArray=double([cen_lon,cen_lat])

        openw,1,'/tmp/coordsToConvert.txt'
        printf,1,utmArray
        close,1

        spawn,'proj +proj=utm  +zone=13 +ellps=WGS84 /tmp/coordsToConvert.txt >
/tmp/coordsConverted.txt'

        openr,1,'/tmp/coordsConverted.txt'
        readf,1,utmArray
        close,1

        NCDF_VARGET, id,  NCDF_VARID(id, 'Times'), times
        times=string(times)

        NCDF_VARGET, id,  NCDF_VARID(id, 'RAINC'), rainc
        NCDF_VARGET, id,  NCDF_VARID(id, 'RAINNC'), rainnc

        rainInt=rainc+rainnc
        rainInt[*,*,1:*]=rainInt[*,*,1:*]-rainInt[*,*,0:*]

        NCDF_VARGET, id,  NCDF_VARID(id, 'T2'), t2

        t2=t2-273.15

        NCDF_VARGET, id,  NCDF_VARID(id, 'PSFC'), psfc
```

```
psfc = 0.01*psfc

NCDF_VARGET, id,  NCDF_VARID(id, 'U10'), u10
NCDF_VARGET, id,  NCDF_VARID(id, 'V10'), v10

vel=sqrt(v10^2+u10^2)

NCDF_VARGET, id,  NCDF_VARID(id, 'Q2'), q2

vapPres=q2*psfc/0.622
satVapPres=0.611*exp(17.3*t2/(t2+237.3))*10.0

RH=vapPres/satVapPres*100

XC=round((3.2*RH/100.0-2.4)*10*10/8.0)>0
pr=where(rainInt)
if pr[0] ne -1 then XC[pr]=10

dimSize=size(rainInt,/dimensions)

window,0   ; name window # 0 (optional)
loadct,12  ; 16-level Red-Hi Values
           ; loadct,5     color scheme STAND-GAMMA

cd,directoryOut

spawn,'mkdir Rain'
spawn,'mkdir Temperature'
spawn,'mkdir Pressure'
spawn,'mkdir RelativeHumidity'
spawn,'mkdir SkyCover'
spawn,'mkdir Wind'

for i=0,dimSize[2]-1 do begin

        tvscl,xc[*,*,i]
        tvscl,rainInt[*,*,i],198,0
        tvscl,t2[*,*,i],0,198
        tvscl,psfc[*,*,i],198,198
        print,'Writing File for time ',times[i]

        out_nCols=dimSize[0]
        out_nRows=dimSize[1]

        xCoord=dindgen(dimSize[0])*res_lon+utmArray[0]-dimSize[0]/2.0D*res_lon
        yCoord=dindgen(dimSize[1])*res_lat+utmArray[1]-dimSize[1]/2.0D*res_lat

        my_date=times[i]
        my_date=strsplit(my_date,'[-_:]',/regex,/EXTRACT)
        fileMM=my_date[1]
        fileDD=my_date[2]
        fileYY=my_date[0]
        fileHH=my_date[3]

        openw,1,'Rain/p'+fileMM+fileDD+fileYY+fileHH+'.txt'
```

```
printf,1,"ncols             "+strtrim(out_nCols,2)
printf,1,"nrows             "+strtrim(out_nRows,2)
printf,1,"xllcorner         "+strtrim(xCoord[0],2)
printf,1,"yllcorner         "+strtrim(yCoord[0],2)
printf,1,"cellsize "+strtrim(res_lon,2)
printf,1,"NODATA_value          -9999"
printf,1,reverse(rainInt[*,*,i],2),format='('+strtrim(out_nCols,2)+'F10.4)'

close,1

openw,1,'Temperature/TA'+fileMM+fileDD+fileYY+fileHH+'.txt'

printf,1,"ncols             "+strtrim(out_nCols,2)
printf,1,"nrows             "+strtrim(out_nRows,2)
printf,1,"xllcorner         "+strtrim(xCoord[0],2)
printf,1,"yllcorner         "+strtrim(yCoord[0],2)
printf,1,"cellsize "+strtrim(res_lon,2)
printf,1,"NODATA_value          -9999"
printf,1,reverse(t2[*,*,i],2),format='('+strtrim(out_nCols,2)+'F10.4)'

close,1

openw,1,'Pressure/PA'+fileMM+fileDD+fileYY+fileHH+'.txt'

printf,1,"ncols             "+strtrim(out_nCols,2)
printf,1,"nrows             "+strtrim(out_nRows,2)
printf,1,"xllcorner         "+strtrim(xCoord[0],2)
printf,1,"yllcorner         "+strtrim(yCoord[0],2)
printf,1,"cellsize "+strtrim(res_lon,2)
printf,1,"NODATA_value          -9999"
printf,1,reverse(psfc[*,*,i],2),format='('+strtrim(out_nCols,2)+'F10.4)'

close,1
openw,1,'RelativeHumidity/RH'+fileMM+fileDD+fileYY+fileHH+'.txt'

printf,1,"ncols             "+strtrim(out_nCols,2)
printf,1,"nrows             "+strtrim(out_nRows,2)
printf,1,"xllcorner         "+strtrim(xCoord[0],2)
printf,1,"yllcorner         "+strtrim(yCoord[0],2)
printf,1,"cellsize "+strtrim(res_lon,2)
printf,1,"NODATA_value          -9999"
printf,1,reverse(rh[*,*,i],2),format='('+strtrim(out_nCols,2)+'F10.4)'

close,1
openw,1,'SkyCover/XC'+fileMM+fileDD+fileYY+fileHH+'.txt'

printf,1,"ncols             "+strtrim(out_nCols,2)
printf,1,"nrows             "+strtrim(out_nRows,2)
printf,1,"xllcorner         "+strtrim(xCoord[0],2)
printf,1,"yllcorner         "+strtrim(yCoord[0],2)
printf,1,"cellsize "+strtrim(res_lon,2)
printf,1,"NODATA_value          -9999"
printf,1,reverse(xc[*,*,i],2),format='('+strtrim(out_nCols,2)+'F10.4)'

close,1
openw,1,'Wind/US'+fileMM+fileDD+fileYY+fileHH+'.txt'
```

```
                printf,1,"ncols             "+strtrim(out_nCols,2)
                printf,1,"nrows             "+strtrim(out_nRows,2)
                printf,1,"xllcorner         "+strtrim(xCoord[0],2)
                printf,1,"yllcorner         "+strtrim(yCoord[0],2)
                printf,1,"cellsize "+strtrim(res_lon,2)
                printf,1,"NODATA_value          -9999"
                printf,1,reverse(vel[*,*,i],2),format='('+strtrim(out_nCols,2)+'F10.4)'

                close,1

        endfor

endif else begin

        cd,directoryIn

        outputFiles=file_search('*')

    window,0
    loadct,12   ; red = high values

        for i=0,n_elements(outputFiles)-1 do begin

                cd,directoryIn

                id = NCDF_OPEN( outputFiles[i] , /NOWRITE)

                NCDF_ATTGET, id, /GLOBAL, 'CEN_LAT', cen_lat
                NCDF_ATTGET, id, /GLOBAL, 'CEN_LON', cen_lon
                NCDF_ATTGET, id, /GLOBAL, 'DY', res_lat
                NCDF_ATTGET, id, /GLOBAL, 'DX', res_lon
                NCDF_ATTGET, id, /GLOBAL, 'DT', dt
                NCDF_ATTGET, id, /GLOBAL, 'START_DATE', start_date

                utmArray=double([cen_lon,cen_lat])

                openw,1,'/tmp/coordsToConvert.txt'
                printf,1,utmArray
                close,1

                spawn,'proj +proj=utm  +zone=13 +ellps=WGS84 /tmp/coordsToConvert.txt >
/tmp/coordsConverted.txt'

                openr,1,'/tmp/coordsConverted.txt'
                readf,1,utmArray
                close,1

                NCDF_VARGET, id,  NCDF_VARID(id, 'Times'), times
                times=string(times)

                NCDF_VARGET, id,  NCDF_VARID(id, 'RAINC'), rainc
                NCDF_VARGET, id,  NCDF_VARID(id, 'RAINNC'), rainnc

                rainInt=rainc+rainnc
```

```
        if i gt 0 then begin
                id2 = NCDF_OPEN( outputFiles[i-1] , /NOWRITE)
                NCDF_VARGET, id2,  NCDF_VARID(id2, 'RAINC'), rainc_1
                NCDF_VARGET, id2,  NCDF_VARID(id2, 'RAINNC'), rainnc_1

                rainInt_1=rainc_1+rainnc_1

                rainInt=rainInt-rainInt_1
        endif

        NCDF_VARGET, id,  NCDF_VARID(id, 'T2'), t2

        t2=t2-273.15

        NCDF_VARGET, id,  NCDF_VARID(id, 'PSFC'), psfc

        psfc = 0.01*psfc

        NCDF_VARGET, id,  NCDF_VARID(id, 'U10'), u10
        NCDF_VARGET, id,  NCDF_VARID(id, 'V10'), v10

        vel=sqrt(v10^2+u10^2)

        NCDF_VARGET, id,  NCDF_VARID(id, 'Q2'), q2

        vapPres=q2*psfc/0.622
        satVapPres=0.611*exp(17.3*t2/(t2+237.3))*10.0

        RH=vapPres/satVapPres*100

        XC=round((3.2*RH/100.0-2.4)*10*10/8.0)>0
        pr=where(rainInt)
        if pr[0] ne -1 then XC[pr]=10

; window,1  (NOT WORKS)
; loadct,5

        cd,directoryOut

        if i eq 0 then begin
                spawn,'mkdir Rain'
                spawn,'mkdir Temperature'
                spawn,'mkdir Pressure'
                spawn,'mkdir RelativeHumidity'
                spawn,'mkdir SkyCover'
        spawn,'mkdir Wind'
        endif

        dimSize=size(rainInt,/dimensions)

        tvscl,xc
        tvscl,rainInt,198,0
        tvscl,t2,0,198
        tvscl,psfc,198,198
        print,'Writing File for time ',times
```

```
out_nCols=dimSize[0]
out_nRows=dimSize[1]

xCoord=dindgen(dimSize[0])*res_lon+utmArray[0]-dimSize[0]/2.0D*res_lon
yCoord=dindgen(dimSize[1])*res_lat+utmArray[1]-dimSize[1]/2.0D*res_lat

my_date=times
my_date=strsplit(my_date,'[-_:]',/regex,/EXTRACT)
fileMM=my_date[1]
fileDD=my_date[2]
fileYY=my_date[0]
fileHH=my_date[3]

openw,1,'Rain/p'+fileMM+fileDD+fileYY+fileHH+'.txt'

printf,1,"ncols          "+strtrim(out_nCols,2)
printf,1,"nrows          "+strtrim(out_nRows,2)
printf,1,"xllcorner      "+strtrim(xCoord[0],2)
printf,1,"yllcorner      "+strtrim(yCoord[0],2)
printf,1,"cellsize "+strtrim(res_lon,2)
printf,1,"NODATA_value       -9999"
printf,1,reverse(rainInt,2),format='('+strtrim(out_nCols,2)+'F10.4)'

close,1

openw,1,'Temperature/TA'+fileMM+fileDD+fileYY+fileHH+'.txt'

printf,1,"ncols          "+strtrim(out_nCols,2)
printf,1,"nrows          "+strtrim(out_nRows,2)
printf,1,"xllcorner      "+strtrim(xCoord[0],2)
printf,1,"yllcorner      "+strtrim(yCoord[0],2)
printf,1,"cellsize "+strtrim(res_lon,2)
printf,1,"NODATA_value       -9999"
printf,1,reverse(t2,2),format='('+strtrim(out_nCols,2)+'F10.4)'

close,1

openw,1,'Pressure/PA'+fileMM+fileDD+fileYY+fileHH+'.txt'

printf,1,"ncols          "+strtrim(out_nCols,2)
printf,1,"nrows          "+strtrim(out_nRows,2)
printf,1,"xllcorner      "+strtrim(xCoord[0],2)
printf,1,"yllcorner      "+strtrim(yCoord[0],2)
printf,1,"cellsize "+strtrim(res_lon,2)
printf,1,"NODATA_value       -9999"
printf,1,reverse(psfc,2),format='('+strtrim(out_nCols,2)+'F10.4)'

close,1
openw,1,'RelativeHumidity/RH'+fileMM+fileDD+fileYY+fileHH+'.txt'

printf,1,"ncols          "+strtrim(out_nCols,2)
printf,1,"nrows          "+strtrim(out_nRows,2)
printf,1,"xllcorner      "+strtrim(xCoord[0],2)
printf,1,"yllcorner      "+strtrim(yCoord[0],2)
printf,1,"cellsize "+strtrim(res_lon,2)
printf,1,"NODATA_value       -9999"
```

```
                printf,1,reverse(rh,2),format='('+strtrim(out_nCols,2)+'F10.4)'

                close,1
                openw,1,'SkyCover/XC'+fileMM+fileDD+fileYY+fileHH+'.txt'

                printf,1,"ncols             "+strtrim(out_nCols,2)
                printf,1,"nrows             "+strtrim(out_nRows,2)
                printf,1,"xllcorner         "+strtrim(xCoord[0],2)
                printf,1,"yllcorner         "+strtrim(yCoord[0],2)
                printf,1,"cellsize "+strtrim(res_lon,2)
                printf,1,"NODATA_value          -9999"
                printf,1,reverse(xc,2),format='('+strtrim(out_nCols,2)+'F10.4)'

                close,1
                openw,1,'Wind/US'+fileMM+fileDD+fileYY+fileHH+'.txt'
                printf,1,"ncols             "+strtrim(out_nCols,2)
                printf,1,"nrows             "+strtrim(out_nRows,2)
                printf,1,"xllcorner         "+strtrim(xCoord[0],2)
                printf,1,"yllcorner         "+strtrim(yCoord[0],2)
                printf,1,"cellsize "+strtrim(res_lon,2)
                printf,1,"NODATA_value          -9999"
                printf,1,reverse(vel,2),format='('+strtrim(out_nCols,2)+'F10.4)'
                close,1

            ;window,0  (NOT WORKS)
            ;loadct,12
          endfor

endelse

end
```